



Genes

& Development

Volume 27 No. 19

October 1, 2013

A JOURNAL OF CELLULAR AND MOLECULAR BIOLOGY

Tissue-specific roles of cathepsin proteases
in tumorigenesis

Also in this issue:

- Regulating meiotic chromosome segregation
- Effects of H3.3 and H2A.Z histone variants on chromatin structure and gene transcription



Cold Spring Harbor Laboratory Press

G&D 2013

Cathepsin C is a tissue-specific regulator of squamous carcinogenesis

Brian Ruffell,^{1,8,9} Nesrine I. Affara,^{1,8} Lucia Cottone,^{1,2} Simon Junankar,¹ Magnus Johansson,¹ David G. DeNardo,¹ Lidiya Korets,¹ Thomas Reinheckel,³ Bonnie F. Sloane,⁴ Mathew Bogyo,^{5,6} and Lisa M. Coussens^{1,7,9,10}

¹Department of Pathology, University of California at San Francisco, San Francisco, California 94143, USA; ²Autoimmunity and Vascular Inflammation Unit, San Raffaele Scientific Institute, 20132 Milan, Italy; ³Institute for Molecular Medicine and Cell Research, Albert-Ludwigs-University Freiburg, D-79104 Freiburg, Germany; ⁴Department of Pharmacology, Barbara Ann Karmanos Cancer Institute, Wayne State University, Detroit, Michigan 48201, USA; ⁵Department of Pathology, ⁶Department of Microbiology and Immunology, Stanford University School of Medicine, Stanford, California 94305, USA; ⁷Helen Diller Family Comprehensive Cancer Center, University of California at San Francisco, San Francisco, California 94143, USA

Serine and cysteine cathepsin (Cts) proteases are an important class of intracellular and pericellular enzymes mediating multiple aspects of tumor development. Emblematic of these is CtsB, reported to play functionally significant roles during pancreatic islet and mammary carcinogenesis. CtsC, on the other hand, while up-regulated during pancreatic islet carcinogenesis, lacks functional significance in mediating neoplastic progression in that organ. Given that protein expression and enzymatic activity of both CtsB and CtsC are increased in numerous tumors, we sought to understand how tissue specificity might factor into their functional significance. Thus, whereas others have reported that CtsB regulates metastasis of mammary carcinomas, we found that development of squamous carcinomas occurs independently of CtsB. In contrast to these findings, our studies found no significant role for CtsC during mammary carcinogenesis but revealed squamous carcinogenesis to be functionally dependent on CtsC. In this context, dermal/stromal fibroblasts and bone marrow-derived cells expressed increased levels of enzymatically active CtsC that regulated the complexity of infiltrating immune cells in neoplastic skin, development of angiogenic vasculature, and overt squamous cell carcinoma growth. These studies highlight the important contribution of tissue/microenvironment context to solid tumor development and indicate that tissue specificity defines functional significance for these two members of the cysteine protease family.

[*Keywords:* cathepsin C; dipeptidyl peptidase I; skin; carcinogenesis; fibroblasts; leukocytes]

Supplemental material is available for this article.

Received June 19, 2013; revised version accepted August 27, 2013.

Extracellular matrix (ECM) remodeling enzymes are well established as critical mediators of tissue homeostasis and pathogenesis in multiple diseases, most notably cancer (Egeblad and Werb 2002; Balkwill et al. 2005; van Kempen et al. 2006; Lopez-Otin and Matrisian 2007; Affara et al. 2009). More recently, a significant role for the cysteine cathepsin (Cts) family of proteases has emerged in cancer, based largely on experimental studies in mouse models of organ-specific solid tumor development, and as biomarkers for risk prediction in human tumors (Turk et al. 2004; Mohamed and Sloane 2006;

Gocheva and Joyce 2007). Eleven Cts have been identified that are predominantly localized in endolysosomal compartments. Due to their intracellular localization, the physiological impact of Cts proteases during solid tumorigenesis had been hypothesized to relate primarily to their activity in terminal protein degradation as well as the modification and activation of other enzymes (Gocheva and Joyce 2007). Several Cts proteases, however, also exhibit extracellular protease activity as secreted enzymes localized at cell surfaces, thus indicating their potential role in pericellular biology, including direct proteolysis of ECM components (Buck et al. 1992) and adhesion molecules (Gocheva et al. 2006) as well as

⁸These authors contributed equally to this work.

⁹Present address: Department of Cell and Developmental Biology, Knight Cancer Institute, Oregon Health and Science University, 3181 SW Sam Jackson Park Road, Portland, OR 97239, USA.

¹⁰Corresponding author

E-mail coussens@ohsu.edu

Article published online ahead of print. Article and publication date are online at <http://www.genesdev.org/cgi/doi/10.1101/gad.224899.113>.

© 2013 Ruffell et al. This article is distributed exclusively by Cold Spring Harbor Laboratory Press for the first six months after the full-issue publication date (see <http://genesdev.cshlp.org/site/misc/terms.xhtml>). After six months, it is available under a Creative Commons License (Attribution-NonCommercial 3.0 Unported), as described at <http://creativecommons.org/licenses/by-nc/3.0/>.

promotion of angiogenic programs (Shi et al. 2003; Joyce et al. 2004).

A role for Cts in pancreatic islet cell carcinogenesis was previously revealed using RIP1-Tag2 transgenic mice, where treatment of mice with a broad-spectrum Cts inhibitor diminished tumor progression (Joyce et al. 2004). Subsequent studies using RIP-Tag2 mice genetically deficient for individual Cts proteases (e.g., CtsB, CtsL, and CtsS genes) revealed their individual roles in regulating tumor progression (Gocheva et al. 2006). In particular, CtsB and CtsS exert protumorigenic activities during pancreatic islet (Gocheva et al. 2010; Gopinathan et al. 2012), mammary (Vasiljeva et al. 2006), and intestinal carcinogenesis (Gounaris et al. 2008); CtsL, on the other hand, limits intestinal (Boudreau et al. 2007), squamous cell (Dennemarker et al. 2010), and two-stage chemical (Benavides et al. 2012) carcinogenesis but is protumorigenic in pancreatic islet tumors (Gocheva et al. 2006). Thus, individual Cts proteases possess distinct roles during tumor development that are likely guided by characteristics of the tissue and organ microenvironment.

CtsC, also known as dipeptidylpeptidase I, is a lysosomal cysteine-class hydrolase belonging to the papain subfamily. Principally an amino dipeptidase, CtsC cleaves two-residue units in the N terminus of polypeptide chains in a nonspecific manner (Turk et al. 1998) and, unlike other cysteine Cts, exists in a tetrameric structure (Turk et al. 2001) that blocks autoactivation (Dahl et al. 2001). Although individuals with loss-of-function mutations in CtsC manifest prepubertal aggressive periodontitis (Noack et al. 2004), Haim-Monk syndrome (Hart et al. 2000), or Papillon-Lefevre syndrome (Frezzini et al. 2004; Pham et al. 2004), CtsC is also of interest due to its catalytic activation of several leukocyte-derived serine proteases, including granzymes A, B, and C; neutrophil elastase (NE); CtsG; proteinase 3; and mast cell chymase (Pham and Ley 1999; Wolters et al. 2001; Adkison et al. 2002; Mallen-St Clair et al. 2004). CtsC expression by mast cells and neutrophils reduces survival during septic peritonitis (Mallen-St Clair et al. 2004) and limits protection from experimental arthritis (Adkison et al. 2002), respectively, indicating its role as a mediator of inflammation. That said, even though infiltrating leukocytes are important regulators of angiogenic programs during pancreatic islet tumor progression, many of which express CtsC (Joyce et al. 2004), absence of the enzyme during pancreatic islet carcinogenesis was without consequence (Gocheva et al. 2006). However, given its role in regulating arthritis and septic immune responses as well as its ability to activate pro-CtsB *in vitro* (Rowan et al. 1992), we hypothesized a functionally significant role for CtsC in other solid tumors where chronic presence and activation of protumoral leukocytes play a role, e.g., mammary carcinomas of MMTV-polyoma middle T (PyMT) mice (DeNardo et al. 2009) and squamous carcinogenesis in K14-HPV16 mice (Andreu et al. 2010). Whereas CtsB plays a significant role during mammary carcinogenesis (Vasiljeva et al. 2006; Gocheva et al. 2010) and regulates proteome homeostasis in skin (Tholen et al. 2013), absence of CtsB in K14-HPV16 mice was without functional sig-

nificance. In contrast, while increased levels and activity of CtsC were prevalent in both mammary and squamous carcinogenesis, absence of the enzyme in MMTV-PyMT mice had no significant effect on any parameter of mammary tumorigenesis, as opposed to CtsC-deficient K14-HPV16 mice that exhibited retarded development of squamous cell carcinomas (SCCs), thus revealing a functionally significant, distinctive, and nonredundant role of CtsC in mediating squamous carcinogenesis.

Results

Increased CtsC activity during K14-HPV16 skin neoplastic progression and mammary carcinogenesis

Akin to what has been reported for islet cell (Gocheva et al. 2006) and mammary (Vasiljeva et al. 2006) carcinogenesis, we observed increased presence and activity for both CtsB and CtsC during squamous carcinogenesis in K14-HPV16 transgenic mice (Fig. 1A–D). Reciprocally, expression of Stefin A and Stefin B, two endogenous CtsB inhibitors, was reduced (Fig. 1A). Despite this correlation and the importance of CtsB as a regulator of neoplastic progression in other solid tumor types, K14-HPV16 mice deficient in CtsB failed to exhibit any significant changes in characteristics of neoplastic progression (e.g., leukocyte infiltration or complexity, angiogenesis, keratinocyte proliferation, or SCC incidence or grade) as compared with age-matched littermate control mice (Supplemental Fig. S1A–H).

In neoplastic skin, CtsC expression was prominent in both epithelial and dermal compartments (Fig. 1C), with a roughly twofold increase in protein levels (Supplemental Fig. S2A) and a >15-fold increase in enzymatic activity based on use of a selective activity-based probe, FY01 (Fig. 1D; Supplemental Fig. S2A; Yuan et al. 2006). Similarly, CtsC expression and activity were also elevated during mammary carcinogenesis in MMTV-PyMT mice, with mammary tumors exhibiting increased presence of CtsC-positive cells within carcinomas as compared with non-neoplastic mammary tissue (Fig. 1E), paralleling increases in CtsC protein levels and activity (Fig. 1F). Interestingly, CtsC expression and activity were similar in lungs containing metastases as compared with non-tumor-bearing mice (Fig. 1F).

Broad expression of CtsC during squamous and mammary carcinogenesis

To delineate which cell types in neoplastic skin and mammary tissue expressed CtsC, tissue sections of premalignant skin (Fig. 2A) and mammary tumors (Fig. 2B) were examined by immunofluorescent staining. CtsC expression was predominantly localized in CD45⁺ leukocytes, including F4/80⁺ macrophages in both tissues and CD117⁺ dermal mast cells in dysplastic skin. Lower levels of CtsC immunoreactivity was also observed in other stromal cell types, including platelet-derived growth factor α (PDGFR α)-positive cells (likely fibroblasts) in both tissues and smooth muscle actin (SMA)-positive perivascular cells (likely mural cells) in mammary tu-

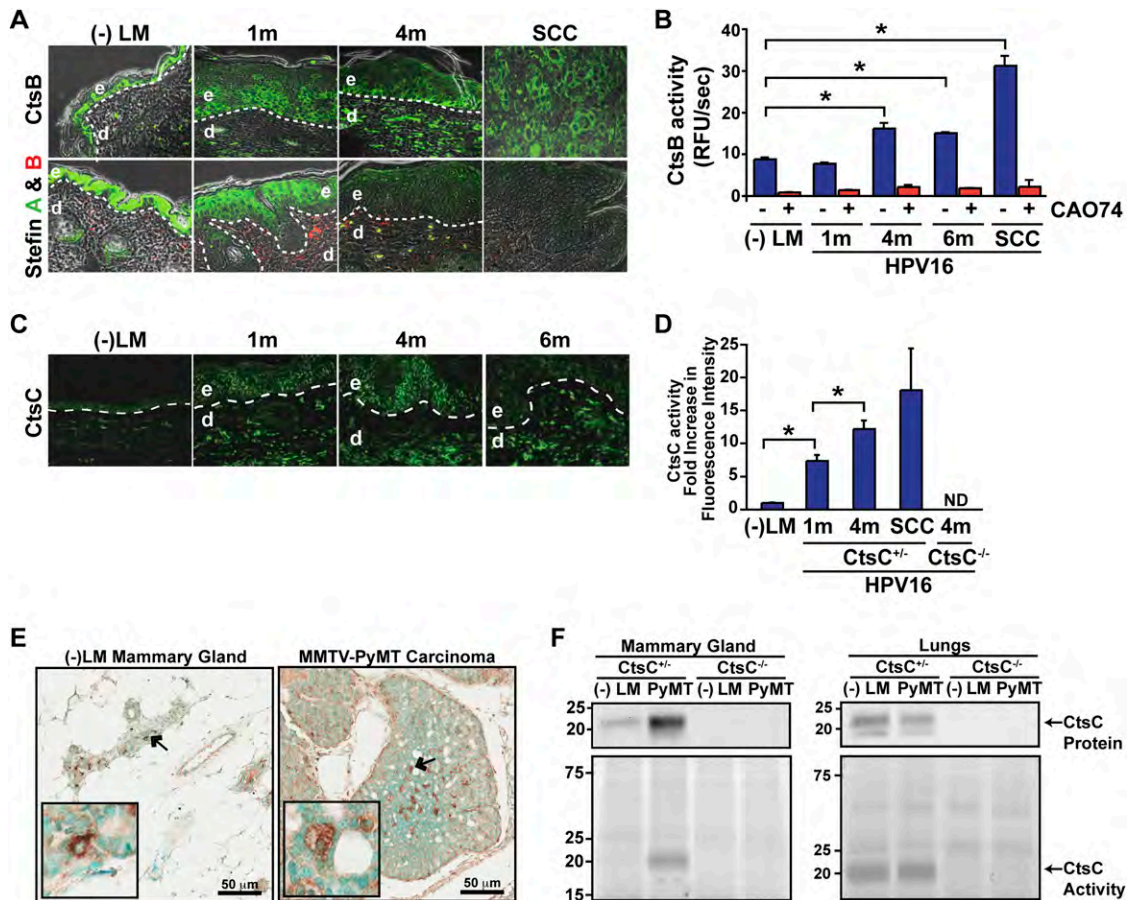


Figure 1. Increased CtsB and CtsC expression and activity during cancer development. (A, top panels) Localization of CtsB expression in skin of congenic negative littermates (–LM), premalignant skin of HPV16 mice at 1 and 4 mo of age, and SCCs as assessed by immunofluorescence staining. (Bottom panels) CtsB endogenous inhibitors, Stefin A, and Stefin B expression in skin of negative littermates (–LM), premalignant skin of HPV16 mice at 1 and 4 mo of age, and SCC tissue. (B) Enzymatic activity of CtsB in whole-tissue lysate as determined by incubation with the fluorogenic substrate Z-Phe-Arg-AMC.HCl. (AMC) 7-Amino-4-methyl coumarin. CtsB-selective inhibitor CAO74 was added to tissue lysates as a control (red bars). $n \geq 3$ mice per group. (C) Immunofluorescent detection of CtsC in negative littermate (–LM) ear skin and hyperplastic (1m), early dysplastic (4m), and late dysplastic (6m) ear tissue of HPV16 mice. (D) Quantitation of FY01 labeling of enzymatically active CtsC within total cell extracts derived from HPV16 ear tissue. $n = 3$ mice per group. (E) Immunodetection of CtsC in representative mammary gland and tumor tissue from CtsC-proficient animals. Arrows mark the areas displayed in the insets. (F, bottom panels) FY01 labeling of active CtsC within total cell extracts from nontransgenic mammary glands (–LM), mammary tumors (PyMT), and normal (–LM) and metastatic (PyMT) lungs. (Top panels) CtsC protein levels were assessed by Western blotting, and CtsC-proficient (CtsC^{+/+}) and CtsC-deficient (CtsC^{–/–}) samples are as indicated. Significance was determined by an unpaired *t*-test; (*) $P < 0.05$.

mors. Similar expression patterns were observed by PCR (Supplemental Fig. S3). Analysis of metastatic foci in the lungs of MMTV-PyMT mice localized CtsC expression to F4/80⁺ macrophages, with minimal expression in other stromal populations (Supplemental Fig. S4). In addition to expression of CtsC by stromal cells, CtsC was expressed at low levels by keratin-positive epithelial cells in skin (Figs. 1A, 2A), mammary tumors (Fig. 2B), and metastatic mammary foci (Supplemental Fig. S4). Using The Human Protein Atlas (Uhlen et al. 2010; <http://www.proteinatlas.org>) we observed similar CtsC expression characteristics in human SCCs and breast carcinomas, with pronounced expression in tumor stroma and low expression levels in most carcinoma cells (Supplemental Fig. S45A,B). Fur-

thermore, immunoreactivity for CtsC was observed in both CD45⁺ and CD68⁺ cells (a macrophage often used to mark human macrophages but also expressed by other stromal cell types) (Fig. 2C; Ruffell et al. 2012) as well as in elongated CD45[–] stromal cells (presumably fibroblasts).

CtsC deficiency limits parameters of neoplastic progression in skin but not mammary tumors

Given the predominant expression of CtsC by infiltrating immune cells and the significant role that infiltrating leukocytes play in regulating both squamous and mammary carcinogenesis (Coussens et al. 1999; Lin et al. 2001; de Visser et al. 2005; Gocheva et al. 2006, 2010; DeNardo

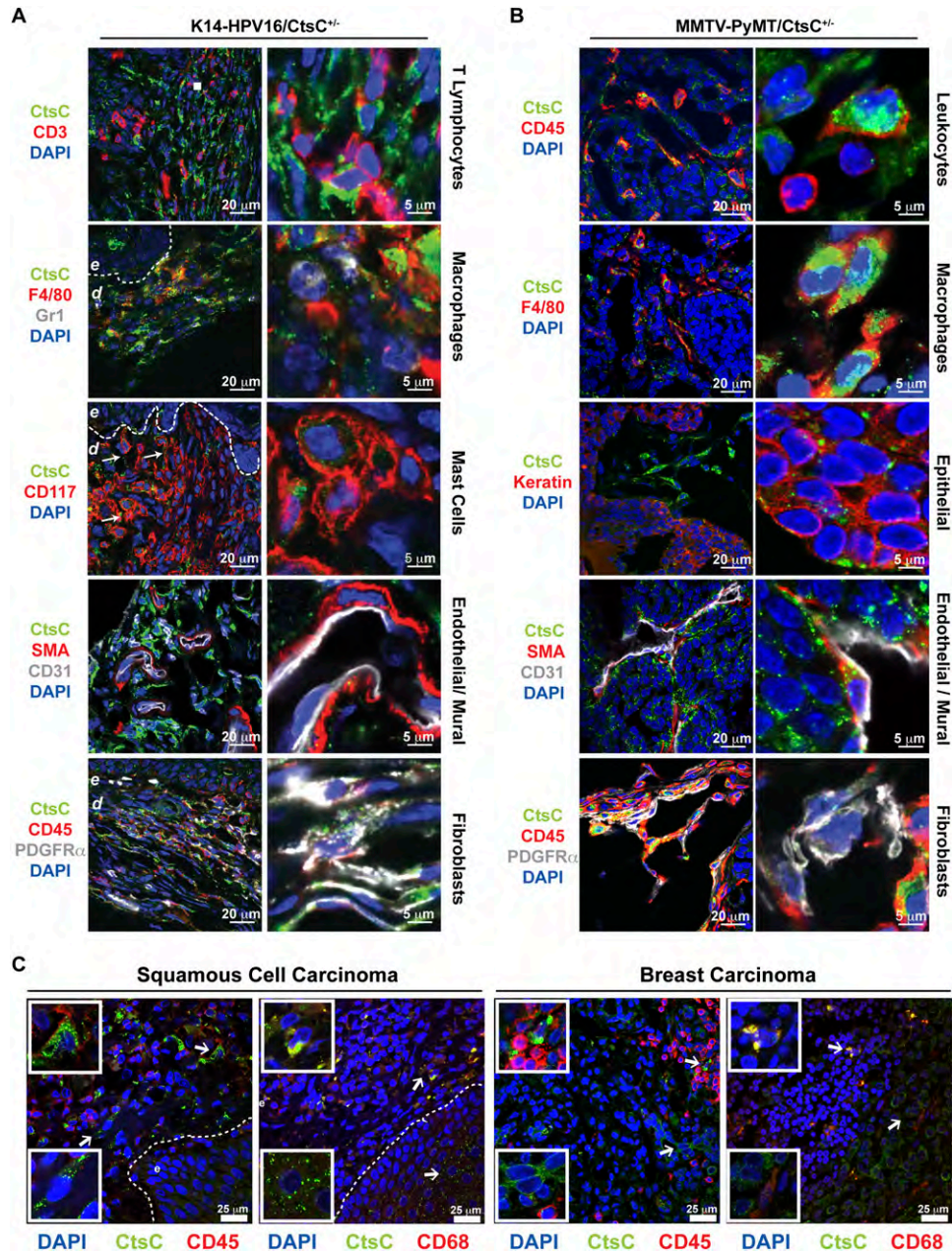


Figure 2. Stromal and epithelial cells express CtsC. Localization of CtsC (green) within dysplastic skin of HPV16/CtsC^{+/-} mice (6 mo of age) (A) and mammary tumors from MMTV-PyMT mice (B). CtsC was highly expressed in F4/80⁺ macrophages, CD45⁺ PDGFR α ⁺ fibroblasts, and epithelial cells in both transgenic models. While CtsC was also expressed by CD31⁺ endothelial cells and SMA⁺ pericytes in mammary tumors, CtsC localization was prominent in CD117⁺ mast cells in HPV16/CtsC^{+/-} ear tissue. (C) Immunofluorescent confocal microscopy of human skin SCCs and breast tumors revealing CtsC expression (green) in the stromal compartment, which colocalized to infiltrating CD45⁺ immune cells and CD68⁺ macrophages (red), in addition to localization to the epithelial compartment of tumors. (Dashed line) Epithelial–dermal interface; (e) epidermis.

et al. 2009, 2011; Andreu et al. 2010; Shree et al. 2011), we examined total leukocyte infiltration and complexity in neoplastic tissue of CtsC-deficient versus CtsC-proficient/HPV16 and PyMT mice. In premalignant skin, CtsC deficiency was associated with reduced levels of infiltrating CD45⁺ cells (Fig. 3A), primarily reflecting reductions in CD11b⁺Gr1⁺ myeloid cells (Fig. 3B), neutrophils (Supplemental Fig. S6A), and mast cells (Supplemental Fig. S6B).

This was accompanied by a relative increase in the proportion of CD11b⁺Gr1⁻ cells, which we previously reported to include F4/80⁺ macrophages and CD11c⁺ dendritic cells (Andreu et al. 2010). These changes in overall immune cell infiltration and complexity were similar to our previously published results with B-cell-deficient or FcR γ -deficient/HPV16 mice (Andreu et al. 2010), indicating a possible functional role for leukocyte-derived CtsC during SCC

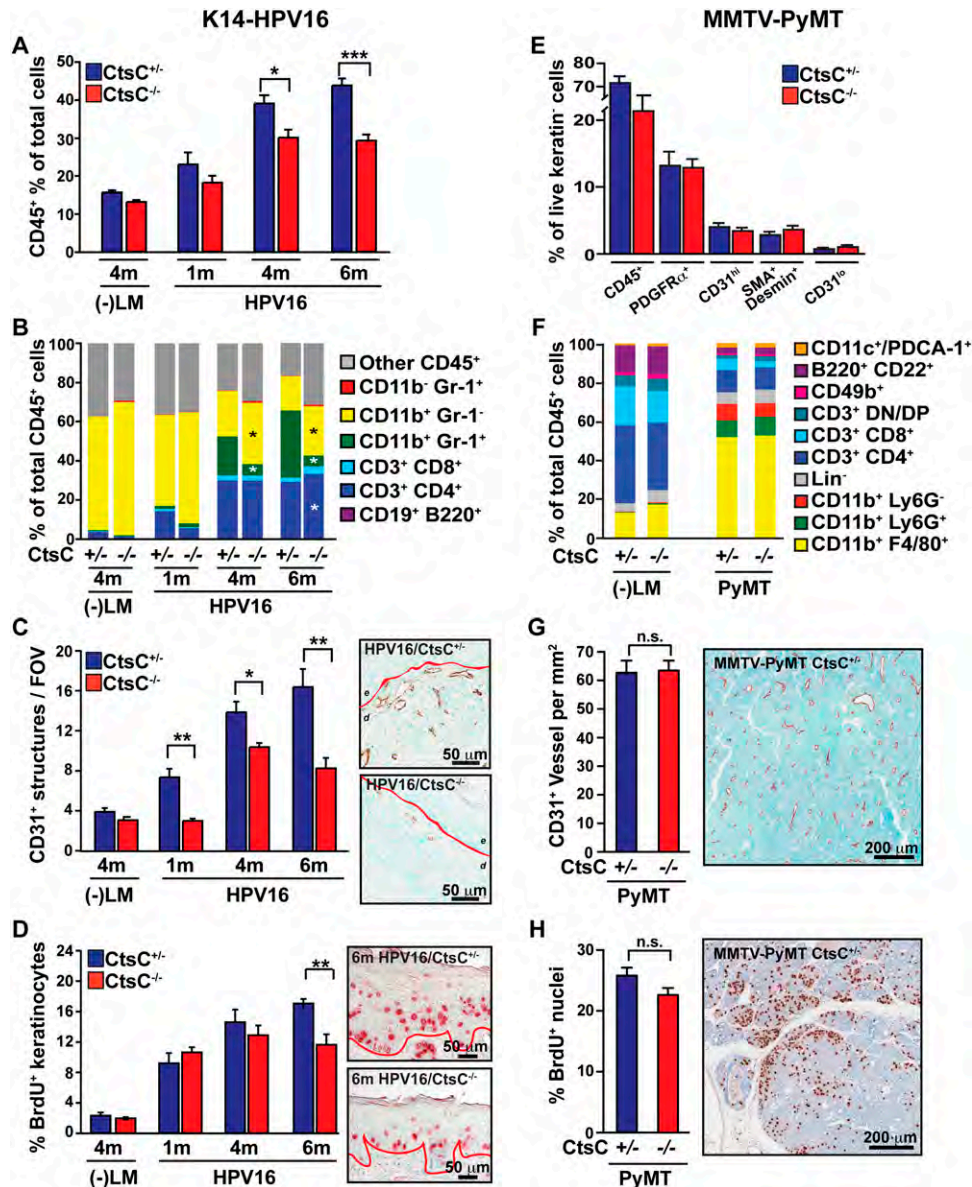


Figure 3. Reduced leukocyte infiltration, angiogenesis, and proliferation in the absence of CtsC in dysplastic HPV16 skin but not mammary tumors. (A) Percentage of CD45⁺ cells in single-cell suspensions isolated from negative littermates (-LM) and HPV16/CtsC^{+/-} (blue) and HPV16/CtsC^{-/-} (red) mice at 1, 4, and 6 mo of age as determined by flow cytometry. *n* = 3–12 mice per group. (B) Composition of immune cell lineages expressed as percentages of total CD45⁺ leukocyte infiltrates in ear tissue of negative littermates (-LM) and HPV16/CtsC^{+/-} and HPV16/CtsC^{-/-} mice at 1, 4, and 6 mo of age as determined by flow cytometry. *n* = 3–10 mice per group. (C) Angiogenic vasculature in skin tissue sections of negative littermates (-LM) and HPV16/CtsC^{+/-} and HPV16/CtsC^{-/-} mice at 1, 4, and 6 mo of age as assessed by CD31 immunohistochemistry revealing endothelial cells (brown staining). Values reflect average number of CD31⁺ vessels from five high-power fields per mouse and four to eight mice per category. Representative images of HPV16/CtsC^{+/-} and HPV16/CtsC^{-/-} mice at 6 mo of age are shown. (Dashed line) Epithelial-dermal interface; (e) epidermis; (d) dermis; (c) cartilage. (D) Quantitative analysis of keratinocyte proliferation as assessed by determining the percentage of BrdU-positive keratinocytes (red staining) at distinct stages of premalignant progression in ear tissue of HPV16/CtsC^{+/-} and HPV16/CtsC^{-/-} mice at 1, 4, and 6 mo of age. Representative images of HPV16/CtsC^{+/-} and HPV16/CtsC^{-/-} mice at 6 mo of age are shown. *n* = 4–7 mice per group. (E) The stromal composition of mammary tumors determined by polychromatic flow cytometry through analysis of the cytokeratin negative populations in MMTV-PyMT/CtsC^{+/-} (blue) versus CtsC^{-/-} (red) animals. *n* = 5–8 mice per group. (F) Composition of CD45⁺ leukocytes within mammary glands isolated from negative littermates (-LM) and mammary tumors from MMTV-PyMT animals as determined by polychromatic flow cytometry. *n* = 7–10 mice per group. (G) Immunohistochemical analysis of tumor angiogenesis as shown by total CD31 vessel density for MMTV-PyMT/CtsC^{+/-} (blue) and MMTV-PyMT/CtsC^{-/-} (red) animals on day 95. *n* = 17–23 mice per group. Representative staining is shown at the right. (H) Proliferation in MMTV-PyMT mammary tumors as determined by the percentage of nuclei incorporating BrdU. *n* = 17–23 mice per group. Representative staining is shown at the right. Significance was determined by an unpaired *t*-test; (*) *P* < 0.05; (**) *P* < 0.01; (***) *P* < 0.001.

development. Indeed, congruent with the reduced presence of CD45⁺ leukocytes in premalignant skin, angiogenic programming (CD31⁺ blood vessels) (Fig. 3C) and keratinocyte hyperproliferation (epithelial bromodeoxyuridine [BrdU] positivity) were reduced in HPV16/CtsC^{-/-} mice as compared with age-matched littermate controls (Fig. 3D; Supplemental Fig. S6C). In contrast, CtsC deficiency in MMTV-PyMT mice failed to alter the presence of CD45⁺ cells or other stromal cell populations in mammary tumors and normal mammary glands (Fig. 3E,F) and subsequently resulted in no changes in vascular density (Fig. 3G) or proliferating mammary epithelial cells (Fig. 3H).

Squamous, but not mammary, carcinogenesis is CtsC-dependent

Attenuated parameters of premalignant progression in CtsC-deficient/HPV16 mice, including reduced leukocyte infiltration and vascularization as well as impaired ability of keratinocytes to achieve hyperproliferative growth characteristics, culminated in diminished presence of focal dysplastic lesions (Fig. 4A) and reduced overall incidence of invasive carcinoma (27% of HPV16/CtsC-deficient mice developed SCCs by 12 mo of age as compared with the ~50% in HPV16/CtsC-proficient [^{+/-}] mice) (Fig. 4B). Moreover, the distribution of tumors that did develop in HPV16/CtsC^{-/-} mice was instead biased toward more differentiated carcinomas with a lower malignant grade as compared with SCCs from HPV16/CtsC^{+/-} mice (Fig. 4C).

On the other hand, CtsC-deficient MMTV-PyMT mice exhibited no change in tumor incidence (Fig. 4D) or growth (Fig. 4E), consistent with the absence of altered stromal cell characteristics in mammary carcinogenesis. Although F4/80⁺ macrophages expressed high levels of CtsC in mammary tumors and macrophages play a significant role in regulating pulmonary metastasis in MMTV-PyMT mice (Lin et al. 2001; DeNardo et al. 2009), there was no change in total metastatic tumor burden (Supplemental Fig. S7A), presence of circulating carcinoma cells (Supplemental Fig. S7B,C), or ability of CtsC-deficient macrophages to promote *in vitro* invasion of mammary epithelial cells (Supplemental Fig. S7D,E). Together, these data revealed a tissue-specific role for CtsC in squamous, but not mammary, tumor development.

Squamous carcinogenesis is independent of mast cell chymase-4 and NE

As a dipeptidase, CtsC is thought to largely function as an activator of other proteases, including mast cell chymases and NE (Affara et al. 2009). Accordingly, we evaluated enzymatic activities of murine mast cell chymase (mMCP4) (Fig. 4F-H) and NE (Fig. 4I-K) in neoplastic tissue derived from HPV16/CtsC^{-/-} mice and revealed an almost complete absence of both serine protease activities, while levels of pro-MMP9 and active MMP9 remained unchanged (Supplemental Fig. S8). Since mMCP4 is the only mast cell chymase expressed in neoplastic skin

of HPV16 mice (Coussens et al. 1999), this result indicated a nonredundant role for CtsC in proteolytic activation of mMCP4 as well as NE. Based on this, we speculated that genetic elimination of either protease might result in phenocopying the attenuated characteristics of neoplastic progression observed in HPV16/CtsC^{-/-} mice. We thus generated cohorts of HPV16/mMCP4^{-/-} (Fig. 4G,H) and HPV16/NE^{-/-} (Fig. 4J,K) mice and evaluated overall SCC incidence as compared with +/- littermate controls. Interestingly, the absence of either mMCP4 or NE had no significant effect on SCC development, indicating that lack of activation of either protease alone was not solely responsible for the observed phenotype in CtsC-deficient/HPV16 mice.

CtsC expression by fibroblasts and leukocytes is necessary for sustained angiogenesis and tumor development

Using syngeneic SCC cell lines (PDSC5.6 and PDSC5.2) originally derived from poorly differentiated SCCs on HPV16 transgenic mice, we previously reported that growth of orthotopic SCCs is significantly diminished in syngeneic mice lacking activating Fcγ receptors on myeloid cells (Andreu et al. 2010). Consistent with this, growth of both PDSC5 cell lines was significantly retarded in syngeneic CtsC^{-/-} mice (Fig. 5A; Supplemental Fig. S9A) despite PDSC5-derived expression of CtsC (Supplemental Fig. S9B), thus indicating a significant role for host-derived CtsC. As with the attenuated development of angiogenic vasculature in HPV16/CtsC^{-/-} mice, vasculature in PDSC5 tumors was significantly reduced as early as day 6 following transplantation into CtsC^{-/-} hosts (Fig. 5B; Supplemental Fig. S9C). Similarly, PDSC5.6 cells failed to promote angiogenic responses in CtsC-deficient hosts using a Matrigel plug assay (Supplemental Fig. S9D).

To delineate the identity of functionally significant CtsC-expressing dermal cells mediating angiogenesis and tumor growth characteristics, we evaluated the two major stromal populations within premalignant skin of HPV16 mice; e.g., CD45⁺ leukocytes and neoplasia-associated fibroblasts (NAFs) (Erez et al. 2010). When coimplanted along with PDSC5 cells in CtsC-proficient hosts, bone marrow-derived (BMD) CD45⁺ cells derived from CtsC-proficient, but not CtsC-deficient, donors fostered rapid tumor growth (Fig. 5C), with BMD mast cells displaying a partial dependence on CtsC for promoting human umbilical vein endothelial cell (HUVEC) migration *in vitro* (Fig. 5D). However, CtsC-proficient BMD CD45⁺ cells failed to rescue tumor growth in CtsC^{-/-} mice (Fig. 5C); thus, we hypothesized that fibroblast-derived CtsC was significant for SCC growth. To assess this, we derived NAFs from hyperplastic and dysplastic skin of HPV16/CtsC^{+/-} mice at 1 and 4 mo of age, respectively, as compared with similar cells derived from age-matched HPV16/CtsC^{-/-} cohorts and monitored PDSC5 tumor growth in syngeneic CtsC^{-/-} versus CtsC^{+/-} mice. While coimplanted NAFs derived from 1-mo-old HPV16/CtsC^{+/-} mice failed to rescue PDSC5

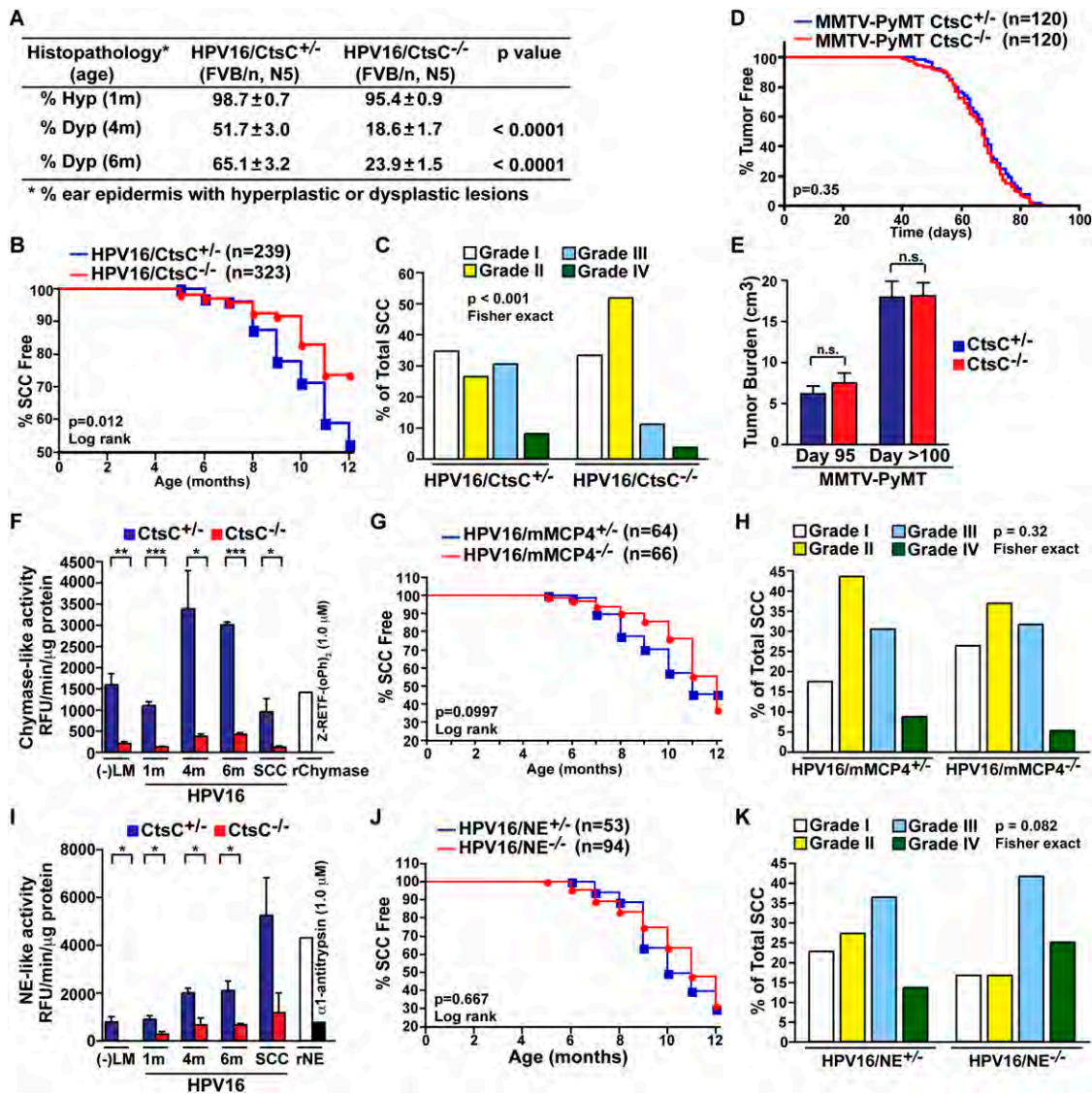


Figure 4. CtsC promotes progression of SCCs but not mammary carcinomas. (A) Percentages of ear skin (area) exhibiting hyperplasia by 1 mo of age (Hyp) or dysplasia by 4 and 6 mo of age (Dys). $n = 9$ – 29 mice per category. (B) Percentage of SCC-free in HPV16/CtsC^{+/-} (blue) and HPV16/CtsC^{-/-} (red) cohorts. (C) Grading of SCC tumors from HPV16/CtsC^{+/-} (right) and HPV16/CtsC^{-/-} (left) mice. $n = 239$ mice (HPV16/CtsC^{+/-} cohorts); $n = 323$ mice (HPV16/CtsC^{-/-} cohorts). (D) Mammary tumor incidence for MMTV-PyMT/CtsC^{+/-} (blue) and MMTV-PyMT/CtsC^{-/-} (red) animals shown by the percentage of mice without visible tumors. $n = 120$ mice per group. (E) Total tumor burden for mice at day 95 and at end stage (day >100). $n = 18$ – 23 mice per group. (F) Enzyme activity of chymase was assessed in skin ear tissue lysates from negative littermates (-LM), HPV16/CtsC^{+/-} (blue) and HPV16/CtsC^{-/-} (red) cohorts at 1, 4, and 6 mo of age; and SCC tumor tissue. $n = 3$ – 4 mice per group, with each sample assayed in triplicate. Significance was determined by an unpaired *t*-test; (*) $P < 0.05$; (**) $P < 0.01$; (***) $P < 0.001$. (G,H) Percentage of SCC-free (G) and SCC tumor grading (H) in HPV16/mMCP4^{-/-} cohorts (red) compared with HPV16/mMCP4^{+/-} control cohorts (blue). $n = 64$ mice (HPV16/mMCP4^{+/-} cohorts); $n = 66$ mice (HPV16/mMCP4^{-/-} cohorts). (I) Enzyme activity of NE was assessed in skin ear tissue lysates from negative littermates (-LM), HPV16/CtsC^{+/-} (blue) and HPV16/CtsC^{-/-} (red) cohorts at 1, 4, and 6 mo of age; and SCC tumor tissue. $n = 3$ mice per group, with each sample assayed in triplicate. Significance was determined by an unpaired *t*-test; (*) $P < 0.05$. (J,K) Percentage of SCC-free (J) and SCC tumor grading (K) in HPV16/NE^{-/-} cohorts (red) compared with HPV16/NE^{+/-} control cohorts (blue). $n = 53$ mice (HPV16/NE^{+/-} cohorts); $n = 94$ mice (HPV16/NE^{-/-} cohorts).

tumor growth in CtsC^{-/-} recipient hosts (Supplemental Fig. S9E), NAFs derived from dysplastic skin of 4-mo-old HPV16/CtsC^{+/-} mice restored early PDSC5 growth kinetics in CtsC^{-/-} mice (Fig. 5E). These findings were in parallel with the *in vitro* and *in vivo* angiogenic potential of NAFs, with only NAFs derived from 4-mo-old HPV16/

CtsC^{+/-} mice able to promote *in vitro* HUVEC migration (Fig. 5F) and vessel formation when implanted as Matrigel plugs (Supplemental Fig. S9F). The altered angiogenic potential of NAFs at 1 and 4 mo of age was not due to changes in *CtsC* expression levels, as this was similar at the two time points (Supplemental Fig. S9G).

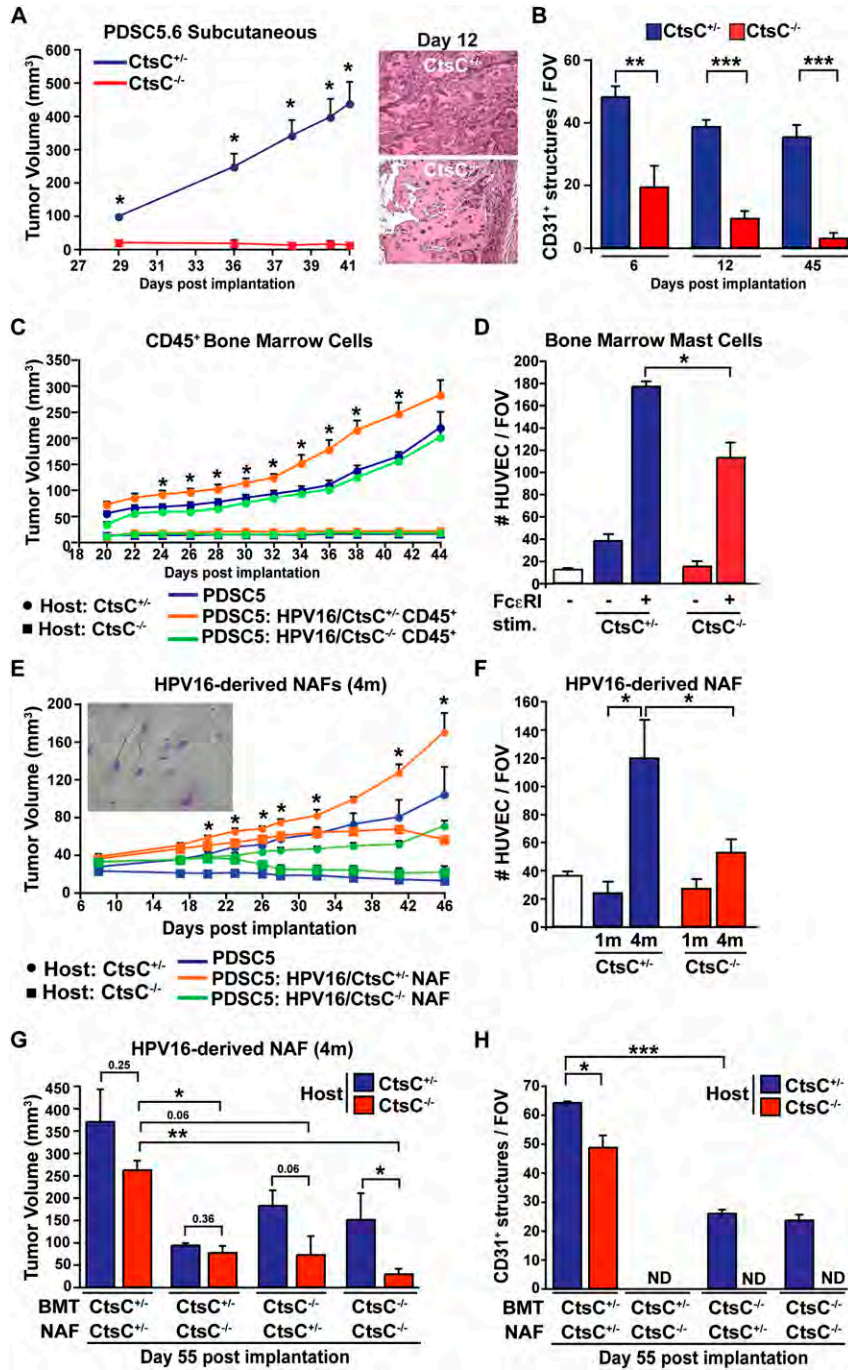


Figure 5. CtsC expression by fibroblasts and immune cells mediates angiogenesis and growth of transplantable tumors. (A) Deficient tumor growth in mice lacking CtsC. PDSC5 clone 6 (PDSC5.6) tumor cells were injected subcutaneously (s.c.) into CtsC^{-/-} versus CtsC^{+/+} syngeneic FVB/n mice. *n* = 20 mice per group. Significance between CtsC^{-/-} versus CtsC^{+/+} hosts was determined by an unpaired *t*-test; (*) *P* < 0.05. (B) Angiogenesis was attenuated as early as 6 d following implantation of PDSC5.6 tumor cells in CtsC^{-/-} mice compared with CtsC^{+/+} cohorts. Blood vessels were evaluated by CD31 immunohistochemistry. Values represent the average of five high-power fields of view per mouse. *n* = 4–14 tumors per category. Significance was determined by an unpaired *t*-test; (**) *P* < 0.01; (***) *P* < 0.001. (C) PDSC5.6 cells alone (blue) or admixed with BMD CD45⁺ isolated from HPV16/CtsC^{+/+} (orange) or HPV16/CtsC^{-/-} (green) mice at 4 mo of age were injected s.c. into CtsC^{+/+} (circle) or CtsC^{-/-} (square) at a ratio of 3:1 (PDSC5:CD45⁺). *n* = 8–9 mice per category. Significance between PDSC5 cells in combination with CD45⁺ derived from HPV16/CtsC^{+/+} versus PDSC5 cells alone in CtsC^{+/+} hosts was determined by an unpaired *t*-test; (*) *P* < 0.05. (D) Mast cells derived from CtsC^{+/+} and CtsC^{-/-} bone marrow and treated for IgE-dependent FcεRI stimulation were evaluated for HUVEC migration using a Boyden chamber assay. *n* = 3–4 mice per group. Significance was determined by an unpaired *t*-test; (*) *P* < 0.05. (E) HPV16/CtsC^{+/+}-derived NAFs isolated at 4 mo of age are necessary but not sufficient to mediate tumor growth in CtsC^{-/-} mice. PDSC5.6 cells alone (blue) or admixed with HPV16/CtsC^{+/+}-derived (orange) or HPV16/CtsC^{-/-}-derived (green) NAFs were injected s.c. into CtsC^{+/+} (circle) or CtsC^{-/-} (square) at a ratio of 3:1 (PDSC5:NAF). *n* = 5–14 mice per group. Significance between PDSC5 cells in combination with NAFs derived from HPV16/CtsC^{+/+} versus PDSC5 cells alone in CtsC^{+/+} hosts was determined by an unpaired *t*-test; (*) *P* < 0.05. (F) HPV16/CtsC^{+/+}-derived and HPV16/CtsC^{-/-}-derived NAFs at 1 and 4 mo of age were evaluated for HUVEC migration using a Boyden chamber assay. *n* = 3–5 mice

per group; samples were assayed in triplicates. Significance was determined by an unpaired *t*-test; (*) *P* < 0.05. (G) Reconstitution of CtsC-deficient mice with CtsC^{+/+} bone marrow in combination with HPV16/CtsC^{+/+}-derived NAFs isolated at 4 mo of age was sufficient to restore and sustain tumor growth in the absence of host-derived CtsC. PDSC5.6 cells were admixed with HPV16/CtsC^{+/+}-derived or HPV16/CtsC^{-/-}-derived NAFs (ratio 3:1) and injected s.c. into CtsC^{+/+} (blue) or CtsC^{-/-} (red) host mice that were lethally irradiated and transplanted with bone marrow from CtsC^{+/+} or CtsC^{-/-} mice that also expressed GFP under control of the β-actin promoter. Shown are tumor volumes at day 55 after tumor cell inoculation. *n* = 3–5 mice per group. Significance was determined by an unpaired *t*-test; (*) *P* < 0.05; (**) *P* < 0.01. (H) Density of angiogenic vasculature from G was evaluated by CD31 immunohistochemistry. Values represent the average of five high-power fields of view per mouse. *n* = 3–5 tumors per category. Significance was determined by an unpaired *t*-test; (*) *P* < 0.05; (***) *P* < 0.001.

Despite their angiogenic potential, PDSC5 tumors rescued by coimplantation with CtsC-proficient NAFs regressed at later stages of tumor growth (Fig. 5E), in-

dicating that while CtsC-proficient NAFs were crucial for initial SCC proliferation in CtsC^{-/-} hosts, they were not sufficient to sustain ongoing tumor development. We

thus reasoned that a combination of CtsC-expressing CD45⁺ leukocytes and dysplasia-derived NAFs might fully restore and sustain PDSC5 tumor development in CtsC^{-/-} recipient mice. We therefore lethally irradiated CtsC^{+/-} and CtsC^{-/-} mice and reconstituted their bone marrow with BMD cells from either CtsC^{+/-} or CtsC^{-/-} donor mice carrying an actin green fluorescent protein (GFP) (Supplemental Fig. S9H) followed by cotransplantation with PDSC5 cells and NAFs derived from either 4-mo-old HPV16/CtsC^{+/-} or HPV16/CtsC^{-/-} mice. As shown in Figure 5G and Supplemental Figure S9I, following transplantation with CtsC^{+/-} BMD cells, HPV16/CtsC^{+/-}-derived NAFs promoted and sustained PDSC5 tumor growth in CtsC^{-/-} mice analogous to control CtsC^{+/-} mice. Sustained tumor growth in CtsC^{-/-} hosts receiving CtsC-proficient bone marrow and NAFs was marked by nearly equivalent vascular density (Fig. 5H), indicating that CtsC expression from both leukocytes and NAFs is required for fostering angiogenic programming and ongoing tumor development.

Discussion

Cathepsin proteases have emerged as functionally significant regulators of several solid tumor types (Joyce and Hanahan 2004; Mason and Joyce 2011) and have thus fueled renewed interest in development of selective protease inhibitors for anti-cancer therapy (Egeblad and Werb 2002; Turk 2006; Fonovic and Bogyo 2007; Palermo and Joyce 2008). This interest has included development of several selective Cts inhibitors, including a covalent CtsC inhibitor with potential for in vivo use (Yuan et al. 2006). Tissue specificity is a significant determinant of expression and activity for multiple classes of proteolytic enzymes, an issue that befuddled clinical trials of matrix metalloproteinase (MMP) inhibitors (Coussens et al. 2002). For example, whereas CtsL is a regulator of proteolytic networks in the skin (Tholen et al. 2013) and is protective against squamous cell (Dennemarker et al. 2010; Benavides et al. 2012) and two-stage chemical (Benavides et al. 2012) carcinogenesis, CtsL is critical for pancreatic islet tumor growth (Gocheva et al. 2006). Based on this, it is now clear that understanding not only temporal dynamics of protease function but also organ specificity in which individual proteases exert functional capacity is of paramount importance for clinical translation.

Along these lines, we evaluated two members of the Cts family, CtsB and CtsC, for their differential contributions to squamous and mammary cancer development. CtsB plays a significant role in de novo carcinogenesis in MMTV-PyMT mice, where it regulates macrophage-mediated primary tumor latency and pulmonary metastasis (Vasiljeva et al. 2006; Gocheva et al. 2010) as well as in glioblastoma (Gondi et al. 2004) and pancreatic islet carcinogenesis (Gocheva et al. 2006). CtsB also regulates the homeostatic proteome in skin (Tholen et al. 2013); however, during squamous carcinogenesis, in spite of increased expression and activity, CtsB exerted no functional role in regulating SCC progression or development

in K14-HPV16 mice. In contrast, whereas CtsC plays a significant role in regulating mammary gland branching morphogenesis (Lilla and Werb 2010) and activates several other proteases in that tissue (Pham and Ley 1999; Wolters et al. 2001; Adkison et al. 2002; Mallen-St Clair et al. 2004), CtsC was not found to play a functional role during mammary carcinogenesis. During squamous carcinogenesis, however, CtsC expression significantly regulated progression to malignancy and overt SCC development, thus identifying CtsC as a significant regulator of carcinogenesis in that locale. Notably, while multiple data sets in Oncomine (<http://www.oncomine.org>; Rhodes et al. 2004) revealed no increase in *CTSC* expression in human breast cancer as compared with counterpart normal tissue (data not shown), SCCs of the oral cavity, nasopharyngeal, thyroid, head and neck, and tongue exhibit significantly increased *CTSC* expression as compared with normal counterpart tissue (Supplemental Fig. S10).

Cumulatively, these studies highlight a tissue-specific role for cathepsin proteases during carcinogenesis. Tissue specificity need not derive from an interaction with the tumor stroma; for example, CtsL-deficiency in epithelial cells has been found to enhance proliferation during squamous cell carcinogenesis (Dennemarker et al. 2010) while limiting proliferation during two-stage chemical and pancreatic islet carcinogenesis (Gocheva et al. 2006; Benavides et al. 2012). That said, the majority of Cts are expressed predominantly within the stromal compartment (Joyce et al. 2004), with a demonstrated role for stromal-derived CtsB and CtsS expression in pancreatic islet and mammary carcinogenesis (Gocheva et al. 2006, 2010; Vasiljeva et al. 2006) and, as described here, a role for stromal CtsC in promoting angiogenesis during squamous carcinogenesis and ongoing SCC development. As with CtsB and CtsS, expression of CtsC by BMD cells is important for promoting tumor growth, with BMD mast cells displaying a reduction in their ability to promote angiogenesis in vitro. However, expression by BMD cells was not sufficient for growth of orthotopic SCCs, with only the combination of CtsC-proficient NAFs and BMD cells able to sustain long-term tumor growth. This important stromal dependency by SCCs for sustained tumor development could partially explain the differences between squamous and mammary locales, as tumor progression in MMTV-PyMT mice is resistant to large-scale perturbations in its stromal compartment, such as the almost complete absence of macrophages (Lin et al. 2002; DeNardo et al. 2011), and unlike squamous SCC development (Coussens et al. 1999), there is no evidence of mast cell dependency for development of mammary tumors (Lilla and Werb 2010).

In leukocytes, CtsC regulates activity of several downstream proteases, and, consistent with previous observations, we observed a reduction in mast cell chymase and NE activities in neoplastic skin of K14-HPV16/CtsC^{-/-} mice (Wolters et al. 2001; Adkison et al. 2002). However, genetic deletion of either mMCP4 or NE in K14-HPV16 mice did not phenocopy CtsC-deficient HPV16 mice in terms of SCC progression, incidence, or grading. It may be that only the combined loss of activity from these and

other serine proteases underlies the important role of CtsC in the angiogenic potential of mast cells or other leukocytes or, alternatively, that SCC incidence and progression are more heavily dependent on CtsC expression by NAFs. NAFs have been found to foster tumor growth by not only directly stimulating tumor cell proliferation and remodeling of ECM architecture but enhancing angiogenesis and orchestrating recruitment and activation of immune cells in the tumor microenvironment (Kalluri and Zeisberg 2006; Erez et al. 2010). It is not entirely clear which of these capabilities are mediated by CtsC, as we observed altered immune infiltration, reduced keratinocyte proliferation, and reduced vascularization in CtsC-deficient mice during squamous cell carcinogenesis. However, as a reduction in vascular density was the most prominent of the phenotypes observed and NAFs from CtsC-deficient mice promoted minimal HUVEC migration in vitro, we hypothesize that CtsC expression by NAFs is necessary for their angiogenic potential.

NAF proangiogenic potential was restricted to fibroblast populations derived from dysplastic skin at 4 mo of age as compared with NAFs derived from 1-mo-old mice, indicating that the programming of proangiogenic NAFs may be a later event during progression. In support of this, although fibroblast activation can be detected as early as 1 mo from the hyperplastic skin of K14-HPV16 mice, these NAFs differ substantially from those isolated from dysplastic skin in terms of inflammatory gene expression (Erez et al. 2010). It has been reported that NAF programming is dependent on IL-1 β expression by leukocytes (Erez et al. 2010), and the inhibition of CtsB in myeloid cells can limit release of IL-1 β (Hornung et al. 2008; Bruchard et al. 2013). However, we found no effect of CtsB deficiency in K14-HPV16 mice or evidence of altered IL-1 β activation in whole-tissue lysate from CtsC-deficient mice (data not shown) to support a role for Cts in mediating NAF programming. The majority of well-characterized CtsC substrates are leukocyte-specific, but as CtsC possesses broad specificity (Turk et al. 1998), it may potentially process a distinct array of proteins with fibroblast origin. Interestingly, fibroblast activation protein (FAP), which has been reported to promote tumor development (Cheng et al. 2002; Santos et al. 2009), is a serine protease (Scanlan et al. 1994; Park et al. 1999); however, there is no evidence that CtsC is involved in FAP activation or even that FAP activation requires cleavage. Thus, while CtsC expression by fibroblasts and BMD cells in skin is critical for promoting angiogenesis and tumor growth, the downstream cleavage products within the stromal compartment mediating this effect remain to be determined.

Stromal populations are increasingly targets for anti-neoplastic therapy, with the hope that targeting genetically stable populations will reduce/delay development of acquired resistance. Fibroblasts have been depleted in several studies by targeting FAP (Loeffler et al. 2006; Ostermann et al. 2008), although as recent reports indicate that this may induce severe toxicities due to expression in normal bone marrow and muscle (Roberts et al. 2013; Tran et al. 2013), perhaps inhibiting fibroblast protease activity may prove more efficacious and safe

(Santos et al. 2009). Unfortunately, current CtsC inhibitors exhibit poor pharmacokinetics (Guay et al. 2010), and even the broad-spectrum cysteine Cts inhibitor JPM-OEt exhibits poor bioavailability in mammary carcinomas and lungs when administered systemically (Schurigt et al. 2008). Targeted delivery of CtsC inhibitors to the tumor microenvironment, such as through encapsulation in ferri-liposomes (Mikhaylov et al. 2011), may be the best approach for moving CtsC inhibitors into the clinic, where they may act to inhibit stromal-driven angiogenesis in SCC.

Materials and methods

Animal care and use

FVB/n strain background mice harboring the PyMT transgene under the control of the MMTV promoter (Guy et al. 1992) and early region HPV16 genes under control of the human keratin 14 promoter (Coussens et al. 1996) have been previously described. CtsC-deficient mice (Pham and Ley 1999) and CtsB-deficient mice (Halangk et al. 2000) were backcrossed into the FVB/n strain to N5 and then intercrossed with MMTV-PyMT or K14-HPV16 mice. HPV16/CtsC^{-/-} versus HPV16/CtsC^{+/-} mice were aged to the indicated time points or were euthanized with low body condition scores per Institutional Animal Care and Use Committee (IACUC) guidelines. For MMTV-PyMT animals, mice >100 d of age with a single 2.0-cm tumor were considered end stage and used for analysis of pulmonary metastasis and circulating tumor cells (CTCs), while 95-d-old animals were used for analysis of primary tumors. Tumor latency/incidence and pulmonary metastasis for MMTV-PyMT animals (DeNardo et al. 2009) and characterization of neoplastic stages based on hematoxylin and eosin staining and keratin intermediate filament expression for histologic examination have been reported previously (Coussens et al. 1996; Daniel et al. 2003). Prior to terminal cardiac perfusion with PBS containing 10 U/mL heparin (Sigma-Aldrich), mice were intraperitoneally (i.p.) injected with 50 mg/kg BrdU (Roche) for 90 min. Resected tissues were either fixed with 4% PFA for 4 h, incubated overnight in 30% sucrose, and embedded in optimal cutting temperature (OCT; Sakura Finetek) medium; directly embedded in OCT post-resection; or incubated overnight in formalin prior to ethanol dehydration and paraffin embedding. All mice were maintained within the University of California at San Francisco (UCSF) Laboratory for Animal Care barrier facility, and all experiments involving animals were approved by the UCSF IACUC (AN082829-02E).

Subcutaneous implantation of PDSC5-derived tumors

PDSC5 cells were suspended in 100 μ L of diluted cold growth factor-reduced Matrigel (BD Biosciences) in PBS (1:1) (0.5×10^6 cells) and inoculated subcutaneously (s.c.) in the flanks of 7-wk-old CtsC^{-/-} versus CtsC^{+/-} mice. Transplantable tumors were measured at a 2-d interval using a digital caliper, and tumor volume was calculated using the equation V (mm³) = $a \times b^2/2$, where a is the largest diameter and b is the smallest diameter. In some experiments, PDSC5 cells were admixed with early passage NAFs derived from the ears of HPV16/CtsC^{-/-} versus HPV16/CtsC^{+/-} mice at 1 mo or 4 mo of age at a ratio of 3:1 (PDSC5:NAF). For Matrigel plug assays, PDSC5 cells (1.5×10^6 cells per 100 μ L) were suspended in 300 μ L of growth factor-reduced Matrigel and injected in the ventral side in the groin area of 7-wk-old CtsC^{-/-} versus CtsC^{+/-} mice. Plugs were dissected

out at 26 d following inoculation, and plugs were recovered, fixed in 10% neutral-buffered formalin, and paraffin-embedded. The extent of neovascularization was evaluated by staining with rat anti-mouse CD31 (BioLegend).

Bone marrow transplantation

Female *CstC^{-/-}* and *CtsC^{+/-}* mice (7 wk old) were lethally X-irradiated with 9.0 Gray (Gy). BMD cells were obtained 24 h later from either *CstC^{-/-}* or *CtsC^{+/-}* donor female mice that ubiquitously expressed enhanced GFP by flushing dissected femurs and tibias with PBS. To prepare single-cell suspensions, flushed cells were passed through 70- μ m nylon strainers (Falcon). Nucleated cells (1×10^7) in 100 μ L were transplanted retro-orbitally into lethally irradiated animals. Neomycin (2 mg/mL) and polymyxin B sulfate (100 μ g/mL) were added to ultrafiltered (Milli-Q) drinking water of irradiated mice. To verify engraftment, peripheral blood leukocytes were collected at 2 wk following engraftment and evaluated for expression of GFP by flow cytometry.

Isolation of primary NAFs

Primary NAFs were prepared by mincing hyperplastic and dysplastic ears of HPV16/*CtsC^{-/-}* versus HPV16/*CtsC^{+/-}* mice that have been sterilized in betadine solution followed by extensive washing in PBS. Cells were grown on collagen type I-coated plates (100 μ g/mL; BD Biosciences) in 0.02 N glacial acetic acid and maintained in subconfluent culture in DMEM containing 10% fetal bovine serum (FBS), 50 U/mL penicillin, 50 μ g/mL streptomycin, and 100 μ g/mL fungizone. Alternatively, NAFs (CD45⁻CD31⁻PDGFR α ⁺) were purified by flow cytometry using BD FACSAria cell sorting system from single-cell suspensions prepared from the ears of HPV16/*CtsC^{-/-}* versus HPV16/*CtsC^{+/-}* mice at 1 and 4 mo of age. Purified PDGFR α ⁺ fibroblasts were further maintained in culture as described above and used in subsequent transplantation assay at an early passage.

Flow cytometry

Tissues were resected from cardiac perfused mice and, following manual mincing, incubated for 30 min at 37°C in DMEM (Invitrogen) with 2.0 mg/mL Collagenase A (Roche) and 50 U/mL DNase I (Roche) in addition to 0.5 mg/mL elastase (Worthington) for lungs or 1 mg/mL hyaluronidase (Worthington) for skin. Single-cell suspensions were prepared by filtering through 70- μ m nylon strainers (BD Biosciences). Staining and analysis for mammary tumors (DeNardo et al. 2011) and skin leukocyte infiltrates (Andreu et al. 2010) were performed as described.

Immunohistochemistry

Immunohistochemistry was performed as previously described (Andreu et al. 2010; DeNardo et al. 2011). Mast cells were evaluated using toluidine blue staining on paraffin sections. Briefly, sections were deparaffinized and rehydrated through graded alcohols and water followed by incubation in 0.1% toluidine blue in 0.1% NaCl (pH 2) for 3 min. Slides were dehydrated and cleared through xylenes and coverslipped with cyto seal. Quantitation was done by either manual counting in five high-power (40 \times) fields of view (FOV) per age-matched section or automated quantitative image analysis using the Aperio ScanScope CS Slide Scanner (Aperio Technologies) system with a 20 \times objective to capture whole-slide images followed by analysis of positively stained cells and CD31⁺ vessels assessed with a nuclear default or microvessel default algorithm, respectively.

Endothelial cell chemotaxis assays

HUVEC (American Type Culture Collection [ATCC]) monolayers were harvested and resuspended in F-12K medium (ATCC) supplemented with 1.0% BSA. HUVECs were then seeded at 10^5 cells (100 μ L) onto the top chamber of 8- μ m transwell filters (Corning). The filters were then placed in a 24-well plate that contained 600 μ L of conditioned medium collected from primary PDGFR α ⁺ NAFs purified by flow cytometry using BD FACSAria cell sorting system from single-cell suspensions prepared from the ears of HPV16/*CtsC^{-/-}* versus HPV16/*CtsC^{+/-}* mice at 4 mo of age as well as control and IgE-stimulated BMMC. Addition of chemotactic factors, including 100 ng/mL rVEGF₁₆₅ (R&D Systems) or 10% FBS, to lower chambers served as positive controls. Chambers were incubated for 8 h at 37°C in a CO₂ incubator. Nonmigrating cells were gently removed from the filter surface using cotton swabs. Inserts were fixed in cold methanol followed by incubation with Diff-Quick stain (IMEB, Inc.). Inserts were then mounted with Cyto seal 60 (Thermo Fisher). HUVEC migration to the underside of the transwell membrane was quantitated by enumerating the number of migrated cells in five random fields (100 \times total magnification) per insert.

Statistical analysis

Unless otherwise indicated, values are represented as means \pm SEM, with significance shown as $P < 0.05$ (*), $P < 0.01$ (**), and $P < 0.001$ (***) by an unpaired *t*-test.

Acknowledgments

We thank M Sameni, E.D. Sandoval, and K. Fujikawa for technical assistance, and acknowledge support from the Department of Defense Breast Cancer Research Program (BCRP) to B.R., the American Association for Cancer Research and NCI Post-doctoral Training grants T32-CA09043 to N.I.A. and T32-CA108462 to D.G.D. and grants from the NIH/NCI (R01 CA130980, R01 CA140943, R01 CA155331, and U54 CA163123), the Department of Defense BCRP Era of Hope Scholar and Scholar Expansion Award (W81XWH-06-1-0416 and W81XWH-11-1-0702), the Susan G. Komen Foundation (KG111084 and KG110560), and the Breast Cancer Research Foundation to L.M.C.

References

- Adkison AM, Raptis SZ, Kelley DG, Pham CT. 2002. Dipeptidyl peptidase I activates neutrophil-derived serine proteases and regulates the development of acute experimental arthritis. *J Clin Invest* **109**: 363–371.
- Affara NI, Andreu P, Coussens LM. 2009. Delineating protease functions during cancer development. *Methods Mol Biol* **539**: 1–32.
- Andreu P, Johansson M, Affara NI, Pucci F, Tan T, Junankar S, Korets L, Lam J, Tawfik D, DeNardo DG, et al. 2010. FcR γ activation regulates inflammation-associated squamous carcinogenesis. *Cancer Cell* **17**: 121–134.
- Balkwill F, Charles KA, Mantovani A. 2005. Smoldering and polarized inflammation in the initiation and promotion of malignant disease. *Cancer Cell* **7**: 211–217.
- Benavides F, Perez C, Blando J, Contreras O, Shen J, Coussens LM, Fischer SM, Kusewitt DF, Digiovanni J, Conti CJ. 2012. Protective role of cathepsin L in mouse skin carcinogenesis. *Mol Carcinog* **51**: 352–361.
- Boudreau F, Lussier CR, Mongrain S, Darsigny M, Drouin JL, Doyon G, Suh ER, Beaulieu JF, Rivard N, Perreault N. 2007.

- Loss of cathepsin L activity promotes claudin-1 overexpression and intestinal neoplasia. *FASEB J* **21**: 3853–3865.
- Bruchard M, Mignot G, Derangere V, Chalmin F, Chevriaux A, Vegran F, Boireau W, Simon B, Ryffel B, Connat JL, et al. 2013. Chemotherapy-triggered cathepsin B release in myeloid-derived suppressor cells activates the Nlrp3 inflammasome and promotes tumor growth. *Nat Med* **19**: 57–64.
- Buck MR, Karustis DG, Day NA, Honn KV, Sloane BF. 1992. Degradation of extracellular-matrix proteins by human cathepsin B from normal and tumour tissues. *Biochem J* **282**: 273–278.
- Cheng JD, Dunbrack RL Jr, Valianou M, Rogatko A, Alpaugh RK, Weiner LM. 2002. Promotion of tumor growth by murine fibroblast activation protein, a serine protease, in an animal model. *Cancer Res* **62**: 4767–4772.
- Coussens LM, Hanahan D, Arbeit JM. 1996. Genetic predisposition and parameters of malignant progression in K14-HPV16 transgenic mice. *Am J Pathol* **149**: 1899–1917.
- Coussens LM, Raymond WW, Bergers G, Laig-Webster M, Behrendtsen O, Werb Z, Coughley GH, Hanahan D. 1999. Inflammatory mast cells up-regulate angiogenesis during squamous epithelial carcinogenesis. *Genes Dev* **13**: 1382–1397.
- Coussens LM, Fingleton B, Matrisian LM. 2002. Matrix metalloproteinase inhibitors and cancer: Trials and tribulations. *Science* **295**: 2387–2392.
- Dahl SW, Halkier T, Lauritzen C, Dolenc I, Pedersen J, Turk V, Turk B. 2001. Human recombinant pro-dipeptidyl peptidase I (cathepsin C) can be activated by cathepsins L and S but not by autocatalytic processing. *Biochemistry* **40**: 1671–1678.
- Daniel D, Meyer-Morse N, Bergsland EK, Dehne K, Coussens LM, Hanahan D. 2003. Immune enhancement of skin carcinogenesis by CD4⁺ T cells. *J Exp Med* **197**: 1017–1028.
- DeNardo DG, Barreto JB, Andreu P, Vasquez L, Tawfik D, Kolhatkar N, Coussens LM. 2009. CD4⁺ T cells regulate pulmonary metastasis of mammary carcinomas by enhancing protumor properties of macrophages. *Cancer Cell* **16**: 91–102.
- DeNardo DG, Brennan D, Rexhapij E, Ruffell B, Shiao S, Gallagher WM, Wadhani N, Kial SD, Junaid SA, Rugo HS, et al. 2011. Leukocyte complexity in breast cancer predicts overall survival and functionally regulates response to chemotherapy. *Cancer Discov* **1**: 54–67.
- Dennemark J, Lohmuller T, Mayerle J, Tacke M, Lerch MM, Coussens LM, Peters C, Reinheckel T. 2010. Deficiency for the cysteine protease cathepsin L promotes tumor progression in mouse epidermis. *Oncogene* **29**: 1611–1621.
- de Visser KE, Korets LV, Coussens LM. 2005. De novo carcinogenesis promoted by chronic inflammation is B lymphocyte dependent. *Cancer Cell* **7**: 411–423.
- Egeblad M, Werb Z. 2002. New functions for the matrix metalloproteinases in cancer progression. *Nat Rev Cancer* **2**: 161–174.
- Erez N, Truitt M, Olson P, Arron ST, Hanahan D. 2010. Cancer-associated fibroblasts are activated in incipient neoplasia to orchestrate tumor-promoting inflammation in an NF- κ B-dependent manner. *Cancer Cell* **17**: 135–147.
- Fonovic M, Bogoy M. 2007. Activity based probes for proteases: Applications to biomarker discovery, molecular imaging and drug screening. *Curr Pharm Des* **13**: 253–261.
- Frezzini C, Leao JC, Porter S. 2004. Cathepsin C involvement in the aetiology of Papillon-Lefevre syndrome. *Int J Paediatr Dent* **14**: 466–467.
- Gocheva V, Joyce JA. 2007. Cysteine cathepsins and the cutting edge of cancer invasion. *Cell Cycle* **6**: 60–64.
- Gocheva V, Zeng W, Ke D, Klimstra D, Reinheckel T, Peters C, Hanahan D, Joyce JA. 2006. Distinct roles for cysteine cathepsin genes in multistage tumorigenesis. *Genes Dev* **20**: 543–556.
- Gocheva V, Wang HW, Gadea BB, Shree T, Hunter KE, Garfall AL, Berman T, Joyce JA. 2010. IL-4 induces cathepsin protease activity in tumor-associated macrophages to promote cancer growth and invasion. *Genes Dev* **24**: 241–255.
- Gondi CS, Lakka SS, Dinh DH, Olivero WC, Gujrati M, Rao JS. 2004. RNAi-mediated inhibition of cathepsin B and uPAR leads to decreased cell invasion, angiogenesis and tumor growth in gliomas. *Oncogene* **23**: 8486–8496.
- Gopinathan A, Denicola GM, Frese KK, Cook N, Karreth FA, Mayerle J, Lerch MM, Reinheckel T, Tuveson DA. 2012. Cathepsin B promotes the progression of pancreatic ductal adenocarcinoma in mice. *Gut* **61**: 877–884.
- Gounaris E, Tung CH, Restaino C, Maehr R, Kohler R, Joyce JA, Ploegh HL, Barrett TA, Weissleder R, Khazaie K. 2008. Live imaging of cysteine-cathepsin activity reveals dynamics of focal inflammation, angiogenesis, and polyp growth. *PLoS ONE* **3**: e2916.
- Guay D, Beaulieu C, Percival MD. 2010. Therapeutic utility and medicinal chemistry of cathepsin C inhibitors. *Curr Top Med Chem* **10**: 708–716.
- Guy CT, Cardiff RD, Muller WJ. 1992. Induction of mammary tumors by expression of polyomavirus middle T oncogene: A transgenic mouse model for metastatic disease. *Mol Cell Biol* **12**: 954–961.
- Halangk W, Lerch MM, Brandt-Nedelev B, Roth W, Ruthenbuenger M, Reinheckel T, Domschke W, Lippert H, Peters C, Deussing J. 2000. Role of cathepsin B in intracellular trypsinogen activation and the onset of acute pancreatitis. *J Clin Invest* **106**: 773–781.
- Hart TC, Hart PS, Michalec MD, Zhang Y, Firatli E, Van Dyke TE, Stabholz A, Zlotogorski A, Shapira L, Soskolne WA. 2000. Haim-Munk syndrome and Papillon-Lefevre syndrome are allelic mutations in cathepsin C. *J Med Genet* **37**: 88–94.
- Hornung V, Bauernfeind F, Halle A, Samstad EO, Kono H, Rock KL, Fitzgerald KA, Latz E. 2008. Silica crystals and aluminum salts activate the NALP3 inflammasome through phagosomal destabilization. *Nat Immunol* **9**: 847–856.
- Joyce JA, Hanahan D. 2004. Multiple roles for cysteine cathepsins in cancer. *Cell Cycle* **3**: 1516–1519.
- Joyce JA, Baruch A, Chehade K, Meyer-Morse N, Giraudo E, Tsai FY, Greenbaum DC, Hager JH, Bogoy M, Hanahan D. 2004. Cathepsin cysteine proteases are effectors of invasive growth and angiogenesis during multistage tumorigenesis. *Cancer Cell* **5**: 443–453.
- Kalluri R, Zeisberg M. 2006. Fibroblasts in cancer. *Nat Rev Cancer* **6**: 392–401.
- Lilla JN, Werb Z. 2010. Mast cells contribute to the stromal microenvironment in mammary gland branching morphogenesis. *Dev Biol* **337**: 124–133.
- Lin EY, Nguyen AV, Russell RG, Pollard JW. 2001. Colony-stimulating factor 1 promotes progression of mammary tumors to malignancy. *J Exp Med* **193**: 727–740.
- Lin E, Gouon-Evans V, Nguyen A, Pollard J. 2002. The macrophage growth factor CSF-1 in mammary gland development and tumor progression. *J Mammary Gland Biol Neoplasia* **7**: 147–162.
- Loeffler M, Kruger JA, Niethammer AG, Reisfeld RA. 2006. Targeting tumor-associated fibroblasts improves cancer chemotherapy by increasing intratumoral drug uptake. *J Clin Invest* **116**: 1955–1962.
- Lopez-Otin C, Matrisian LM. 2007. Emerging roles of proteases in tumour suppression. *Nat Rev Cancer* **7**: 800–808.

- Mallen-St Clair J, Pham CT, Villalta SA, Caughey GH, Wolters PJ. 2004. Mast cell dipeptidyl peptidase I mediates survival from sepsis. *J Clin Invest* **113**: 628–634.
- Mason SD, Joyce JA. 2011. Proteolytic networks in cancer. *Trends Cell Biol* **21**: 228–237.
- Mikhaylov G, Mikac U, Magaeva AA, Itin VI, Naiden EP, Psakhye I, Babes L, Reinheckel T, Peters C, Zeiser R, et al. 2011. Ferri-liposomes as an MRI-visible drug-delivery system for targeting tumours and their microenvironment. *Nat Nanotechnol* **6**: 594–602.
- Mohamed MM, Sloane BF. 2006. Cysteine cathepsins: Multifunctional enzymes in cancer. *Nat Rev Cancer* **6**: 764–775.
- Noack B, Gorgens H, Hoffmann T, Fanghanel J, Kocher T, Eickholz P, Schackert HK. 2004. Novel mutations in the cathepsin C gene in patients with pre-pubertal aggressive periodontitis and Papillon-Lefevre syndrome. *J Dent Res* **83**: 368–370.
- Ostermann E, Garin-Chesa P, Heider KH, Kalat M, Lamche H, Puri C, Kerjaschki D, Rettig WJ, Adolf GR. 2008. Effective immunoconjugate therapy in cancer models targeting a serine protease of tumor fibroblasts. *Clin Cancer Res* **14**: 4584–4592.
- Palermo C, Joyce JA. 2008. Cysteine cathepsin proteases as pharmacological targets in cancer. *Trends Pharmacol Sci* **29**: 22–28.
- Park JE, Lenter MC, Zimmermann RN, Garin-Chesa P, Old LJ, Rettig WJ. 1999. Fibroblast activation protein, a dual specificity serine protease expressed in reactive human tumor stromal fibroblasts. *J Biol Chem* **274**: 36505–36512.
- Pham CT, Ley TJ. 1999. Dipeptidyl peptidase I is required for the processing and activation of granzymes A and B in vivo. *Proc Natl Acad Sci* **96**: 8627–8632.
- Pham CT, Ivanovich JL, Raptis SZ, Zehnbauser B, Ley TJ. 2004. Papillon-Lefevre syndrome: Correlating the molecular, cellular, and clinical consequences of cathepsin C/dipeptidyl peptidase I deficiency in humans. *J Immunol* **173**: 7277–7281.
- Rhodes DR, Yu J, Shanker K, Deshpande N, Varambally R, Ghosh D, Barrette T, Pandey A, Chinnaiyan AM. 2004. ONCOMINE: A cancer microarray database and integrated data-mining platform. *Neoplasia* **6**: 1–6.
- Roberts EW, Deonarine A, Jones JO, Denton AE, Feig C, Lyons SK, Espeli M, Kraman M, McKenna B, Wells RJ, et al. 2013. Depletion of stromal cells expressing fibroblast activation protein- α from skeletal muscle and bone marrow results in cachexia and anemia. *J Exp Med* **210**: 1137–1151.
- Rowan AD, Mason P, Mach L, Mort JS. 1992. Rat procathepsin B. Proteolytic processing to the mature form in vitro. *J Biol Chem* **267**: 15993–15999.
- Ruffell B, Au A, Rugo HS, Esserman LJ, Hwang ES, Coussens LM. 2012. Leukocyte composition in human breast cancer. *Proc Natl Acad Sci* **109**: 2796–2801.
- Santos AM, Jung J, Aziz N, Kissil JL, Pure E. 2009. Targeting fibroblast activation protein inhibits tumor stromagenesis and growth in mice. *J Clin Invest* **119**: 3613–3625.
- Scanlan MJ, Raj BK, Calvo B, Garin-Chesa P, Sanz-Moncasi MP, Healey JH, Old LJ, Rettig WJ. 1994. Molecular cloning of fibroblast activation protein α , a member of the serine protease family selectively expressed in stromal fibroblasts of epithelial cancers. *Proc Natl Acad Sci* **91**: 5657–5661.
- Schurigt U, Sevenich L, Vannier C, Gajda M, Schwinde A, Werner F, Stahl A, von Elverfeldt D, Becker AK, Bogoy M, et al. 2008. Trial of the cysteine cathepsin inhibitor JPM-OEt on early and advanced mammary cancer stages in the MMTV-PyMT-transgenic mouse model. *Biol Chem* **389**: 1067–1074.
- Shi GP, Sukhova GK, Kuzuya M, Ye Q, Du J, Zhang Y, Pan JH, Lu ML, Cheng XW, Iguchi A, et al. 2003. Deficiency of the cysteine protease cathepsin S impairs microvessel growth. *Circ Res* **92**: 493–500.
- Shree T, Olson OC, Elie BT, Kester JC, Garfall AL, Simpson K, Bell-McGuinn KM, Zabor EC, Brogi E, Joyce JA. 2011. Macrophages and cathepsin proteases blunt chemotherapeutic response in breast cancer. *Genes Dev* **25**: 2465–2479.
- Tholen S, Biniossek ML, Gansz M, Gomez-Auli A, Bengsch F, Noel A, Kizhakkedathu JN, Boerries M, Busch H, Reinheckel T, et al. 2013. Deletion of cysteine cathepsins B or L yields differential impacts on murine skin proteome and degradome. *Mol Cell Proteomics* **12**: 611–625.
- Tran E, Chinnasamy D, Yu Z, Morgan RA, Lee CC, Restifo NP, Rosenberg SA. 2013. Immune targeting of fibroblast activation protein triggers recognition of multipotent bone marrow stromal cells and cachexia. *J Exp Med* **210**: 1125–1135.
- Turk B. 2006. Targeting proteases: Successes, failures and future prospects. *Nat Rev Drug Discov* **5**: 785–799.
- Turk D, Guncar G, Podobnik M, Turk B. 1998. Revised definition of substrate binding sites of papain-like cysteine proteases. *Biol Chem* **379**: 137–147.
- Turk D, Janjic V, Stern I, Podobnik M, Lamba D, Dahl SW, Lauritzen C, Pedersen J, Turk V, Turk B. 2001. Structure of human dipeptidyl peptidase I (cathepsin C): Exclusion domain added to an endopeptidase framework creates the machine for activation of granular serine proteases. *EMBO J* **20**: 6570–6582.
- Turk V, Kos J, Turk B. 2004. Cysteine cathepsins (proteases)—on the main stage of cancer? *Cancer Cell* **5**: 409–410.
- Uhlen M, Oksvold P, Fagerberg L, Lundberg E, Jonasson K, Forsberg M, Zwahlen M, Kampf C, Wester K, Hober S, et al. 2010. Towards a knowledge-based Human Protein Atlas. *Nat Biotechnol* **28**: 1248–1250.
- van Kempen LC, de Visser KE, Coussens LM. 2006. Inflammation, proteases and cancer. *Eur J Cancer* **42**: 728–734.
- Vasiljeva O, Papazoglou A, Kruger A, Brodoefel H, Korovin M, Deussing J, Augustin N, Nielsen BS, Almholt K, Bogoy M, et al. 2006. Tumor cell-derived and macrophage-derived cathepsin B promotes progression and lung metastasis of mammary cancer. *Cancer Res* **66**: 5242–5250.
- Wolters PJ, Pham CT, Muilenburg DJ, Ley TJ, Caughey GH. 2001. Dipeptidyl peptidase I is essential for activation of mast cell chymases, but not tryptases, in mice. *J Biol Chem* **276**: 18551–18566.
- Yuan F, Verhelst SH, Blum G, Coussens LM, Bogoy M. 2006. A selective activity-based probe for the papain family cysteine protease dipeptidyl peptidase I/cathepsin C. *J Am Chem Soc* **128**: 5616–5617.

Cathepsin C is a Tissue-Specific Regulator of Squamous Carcinogenesis

Supplemental Data

Brian Ruffell^{1,6,#}, Nesrine I. Affara^{1,#}, Lucia Cottone^{1,2}, Simon Junankar¹, Magnus Johansson¹, David G. DeNardo¹, Lidiya Korets¹, Thomas Reinheckel³, Bonnie F. Sloane⁴, Mathew Bogyo⁵, and Lisa M. Coussens^{1,6,*}

¹Department of Pathology and ⁶Helen Diller Family Comprehensive Cancer Center, University of California, San Francisco, San Francisco, CA 94143

²Autoimmunity and Vascular Inflammation Unit, San Raffaele Scientific Institute, Milan, Italy

³Institute for Molecular Medicine and Cell Research, Albert-Ludwigs-University Freiburg, Freiburg, Germany

⁴Department of Pharmacology and Barbara Ann Karmanos Cancer Institute, Wayne State University, Detroit, MI 48201

⁵Department of Pathology and Department of Microbiology and Immunology, Stanford University School of Medicine, Stanford, CA 94305-5324

⁶Current address: Department of Cell & Developmental Biology, Knight Cancer Institute, Oregon Health & Sciences University, 3181 SW Sam Jackson Park Road, Portland OR 97239-3098. Email: coussenl@ohsu.edu

#Authors contributed equally to this work

* Address for correspondence:

Lisa M. Coussens, Ph.D.
Cell & Developmental Biology
Knight Cancer Institute
Oregon Health & Science University
Mail Code L215
3181 SW Sam Jackson Park Road
Portland, OR 97239-3098
Voice: 503-494-7811
Fax: 503-494-4253
email: coussenl@ohsu.edu

Running title: Cathepsin C in Carcinogenesis

Key words: cathepsin C, dipeptidyl peptidase I, cathepsin B, mammary, breast, skin, carcinogenesis, fibroblasts, leukocytes

Supplemental Materials and Methods

ELISA

Protein lysates were prepared from PBS-perfused ear tissue for enzyme solution assays. Tissue was pulverized in liquid nitrogen before being homogenized in 8 volumes of lysis buffer containing 0.25 M sucrose, 5 mM Tris (pH 7.5). Samples were centrifuged at 4000 rpm for 30 min, and supernatants (50 μ g of protein) were used for ELISA assays. Sandwich ELISA analyses were performed using antibodies for CtsC, MMP-9, proMMP-9 and TIMP-1 according to manufacturer's instructions (R&D systems). Recombinant protein standards for CtsC, MMP-9, and TIMP-1 (R&D systems) were used to quantify protein levels. ELISA's were developed with OPD (Sigma) in 1 M H₂SO₄ acid stop, and optical density was measured at 490 nm on a SpectraMax 340 spectrophotometer (Molecular Devices).

CtsB activity

Tissue samples from age-matched HPV16 and (-) littermates were snap frozen, weighed, and pulverized in liquid nitrogen, then homogenized in PBS containing 0.1% Triton X-100. Homogenates were spun at 16,000 G for 10 min and supernatants were collected and stored at -20°C. To assess cysteine protease activity, samples (10 μ g) were treated with 100 mM sodium acetate (pH 5.5), 5 mM dithiothreitol (DTT), and the fluorogenic substrate N-Carbobenzyloxy-Phe-Arg-7-amido-4-methylcoumarin (ZFRAMC; 20 μ M), in the presence or absence of the CtsB specific inhibitor Ca074 (1 μ M).

CtsC activity

Cell lysates were prepared from snap frozen tissues using M-PER® Mammalian Protein Extraction Reagent (Thermo Scientific) according to the manufacturer's instructions. Supernatants were passed through Micro Bio-Spin 6 Chromatography buffer exchange columns (Bio-Rad) with 50 mM sodium acetate, 5.0 mM MgCl₂, pH 5.5, and supernatant protein concentration was determined with the DC Protein Assay Kit (Bio-Rad). Samples were adjusted to 1.0 mg/ml total protein concentration and 2.0 mM fresh DTT (Roche) was added to samples prior to incubation with 0.1 μ M of the CtsC activity probe FY01, conjugated to fluorescent Bodipy-TMR-X (Yuan et al. 2006). After 30 min, reactions were quenched by boiling samples for 5 min with 4x SDS sample buffer consisting of 40% glycerol (Sigma Aldrich), 0.2 M Tris/HCl pH 6.8 (Fisher Scientific), 20% β -mercaptoethanol (GIBCO), 12% SDS (Bio-Rad) and 0.4 mg/ml bromophenol blue (Sigma). Equal amounts of protein per lane were resolved by SDS-PAGE (15% acrylamide) along with a molecular weight marker (Odyssey Protein Molecular Weight Marker (LI-COR Biosciences). Fluorescently labeled bands were visualized within gels using a Fluorescent Image Analyzer FLA5100 (Fuji), followed by

protein transfer onto low auto-fluorescent Immobilon FL membranes (Millipore). Membranes were saturated in blocking buffer (LI-COR Biosciences) for 1 hr at room temperature and CtsC was detected by incubating overnight at 4°C with goat anti-mouse CtsC (R&D) diluted 1:1000 in blocking buffer with 0.2% Tween-20, followed by primary antibody detection with donkey-anti-goat-IRDye 800CW (LI-COR Biosciences) diluted 1:12000 in blocking buffer, 0.2% Tween-20, and 0.01% sodium dodecyl sulfate, and visualization of bands using the Odyssey Infrared Imaging System (LI-COR Biosciences).

Immunofluorescent detection of CtsB, Stefin A, and Stefin B

OCT-embedded tissue sections (10- μ m) were air-dried, fixed in acetone for 5 minutes, and subjected to staining as follows: To prevent nonspecific antibody binding, sections were incubated with blocking buffer (PBS containing 5% goat serum and 2.5% BSA). Sections were then incubated with primary antibody rat anti-mouse CtsB (1:100; Caltag CA), rabbit anti-human Stefin A/Cystatin A (1:100; Abcam), and rabbit anti-human Stephin B/Cystatin B (1:100) for 1 hr at room temperature, followed by subsequent incubation with Alexa-conjugated secondary antibodies (1:100, Jackson ImmunoResearch, PA) for 45 minutes. Slides were mounted using Vectashield containing 4',6 diamidino-2-phenylindole (DAPI) (Vector, Burlingame, CA).

Immunofluorescent detection of CtsC

For CtsC localization, 10 μ m sections of PFA fixed, sucrose protected, OCT embedded tissues were thawed at 37°C for 10 minutes, washed with PBS, then permeabilized/blocked for 1 hr with PBS containing 2.5% BSA, 5% Horse Serum, and 0.3% Triton-X100 (Fisher Scientific). Primary antibodies diluted in 0.5x blocking buffer and incubated on sections overnight at 4°C, included: goat anti-mouse CtsC (1:100, R&D), mouse anti- α -smooth muscle actin Cy3 (1:1000, Sigma), rabbit anti-desmin (1:500, Millipore/Upstate), rabbit anti-pankeratin Alexa 488 (1:50, Cell Signaling), and the rat anti-mouse mAbs CD45 (1:100, BioLegend), PDGFR α (1:50 eBioscience), Gr-1 (1:100, eBioscience), CD31 (1:100, BioLegend), CD117 (1:100, BD Biosciences); and biotinylated mAbs CD3, CD45, CD31, F4/80 (1:5000, BioLegend). TSA indirect kit (Perkin Elmer) was used to amplify the signal from biotinylated primary antibodies according to the manufacturer's instructions. After washing, appropriate secondary antibodies from Invitrogen were used at a 1:500 dilution. Slides were mounted with ProLong Gold with DAPI anti-fade mounting medium (Invitrogen) and pictures were taken with a LSM510 Confocal Laser Scanning Microscope (Carl Zeiss). Images were taken with a 63X objective and at an additional 5X digital magnification

For immunofluorescent staining of human SCC and breast cancer tissues, 5 μ m sections of formalin fixed, paraffin embedded tissue were deparaffinized with xylene, rehydrated, and subjected to antigen

retrieval with heated citrate buffer (BioGenex). After 1 hr in horse serum blocking buffer, goat anti-human CtsC (1:100, R&D) and either mouse anti-human CD68 (1:100, KP1, Neomarkers/Thermo Scientific) or mouse anti-human CD45 (1:100, HI30, eBioscience) were then applied overnight at 4°C. After washing, anti-goat Alexa 488 and anti-mouse Alexa 546 (1:500, Invitrogen) were applied for 1 hr, slides were washed three times, and Prolong Gold with DAPI (Invitrogen) was used for mounting. Images were captured with a 20X objective on a Nikon C1si Spectral Confocal Microscope.

Substrate Zymography

Ear samples from (-LM), HPV16/CtsC^{+/-}, and HPV16/CtsC^{-/-} mice at 1, 4, and 6 months of age and SCC (as verified by histological analysis of paraffin-embedded sections) were weighed and then homogenized (1:8 weight to volume) in lysis buffer containing 50 mM Tris-HCL (pH 8.0), 150 mM NaCl, 1% NP-40, 0.5% deoxycholate, and 0.1% SDS. Soluble extracts were prepared by centrifugation and subsequent analysis by gelatin zymography as previously described (Coussens et al. 2000) on 10% SDS-polyacrylamide gels copolymerized with substrate (0.42 mg/ml gelatin) in sample buffer (10% SDS, 0.25 M Tris-HCL, 0.1% Bromophenol blue, pH 6.8). Following electrophoresis, gels were washed in 2% Triton X-100, incubated for 24 hr at 37°C in 50 mM Tris-HCL (pH 8.16) and 10 mM CaCl₂, and stained in 0.5% Coomassie Blue and then destained in 40% methanol and 10% glacial acetic acid. Active bands were located by negative staining.

Chymase, neutrophil elastase and gelatinase activity assays

Protein lysates were prepared from PBS-perfused ear tissue for enzyme solution assays. Tissue was first ground in liquid nitrogen before being lysed in 2 ml homogenizers with 8 volumes of lysis buffer containing 0.25 M sucrose, 5 mM Tris (pH 7.5). Samples were centrifuged at 4000 rpm for 30 min, supernatants were removed, and pellets were further re-extracted with buffer containing 2 M NaCl, 10 mM Bis-Tris (pH 6.1) and centrifuged at 13,000 rpm for 10 min. Supernatants were then collected for the analysis of chymase, neutrophil elastase, and gelatinase activities. Chymase-like activity was measured by addition of 10 µg of sample to assay buffer containing the substrate Suc-Ala-Ala-Pro-Phe-AMC (380 µM; Calbiochem), 1.8 M NaCl, and 10% dimethylsulfoxide in 0.45 M Tris-HCl (pH 8.0), at an excitation of 380 nm and emission of 460 nm. Neutrophil elastase-like activity was measured by addition of 10 µg of sample to assay buffer containing the substrate MeOSuc-AAPV-AMC (240 µM; Calbiochem), 50 mM NaOAc (pH 7.8), and 200 mM NaCl at an excitation of 380 nm and emission of 460 nm. Gelatinase-like activity was measured by the addition of 10 µg of sample to assay buffer containing fluorescein-conjugated DQ Gelatin substrate (2 µg/ml; Molecular Probe) in 50 mM Tris-HCl pH 7.6, 150 mM NaCl, 5 mM CaCl₂, 0.2 mM sodiumazide,

and 0.05% of the detergent Brij35 at an excitation of 485 nm and emission of 530 nm. Fluorescence was measured at 37°C on a SpectraMax Gemini™ spectrophotometer (Molecular Devices) operated by SoftMax Pro 5.0 software (Molecular Devices). Chymase, neutrophil elastase, and gelatinase inhibition was performed in the presence of 1.0 μM Z-RETF-(oPh)₂, 5 μM nafamostat mesylate (Calbiochem), 1 μM a1-antitrypsin, human plasma (Calbiochem), and 4.0 mM 1.10-phenanthroline (Sigma), respectively. Change in Relative Fluorescence Units (RFU)/min/μg tissue protein was determined using SoftMax Pro 5.0 software (Molecular Devices).

Flow cytometry

Tissues were resected from cardiac perfused mice, and following manual mincing, were incubated for 30 min at 37°C in DMEM (Invitrogen) with 2.0 mg/ml Collagenase A (Roche) and 50 U/ml DNase I (Roche), in addition to 0.5 mg/ml of Elastase (Worthington) for lungs or 1 mg/ml Hyaluronidase (Worthington) for skin. Single cell suspensions were prepared by filtering through 70 μm nylon strainers (BD Biosciences). Approximately 10⁶ cells were Fc blocked with 2.0 μg/ml of 2.4G2 in PBS containing Live Dead Aqua (1:500, Invitrogen) for 30 min on ice. A 30 min incubation was then performed in PBS containing 2.0 mM EDTA and 5% fetal calf serum using appropriate combinations of mAbs from eBioscience for 12-parameter flow cytometry: CD45 PE-Cy7 (1:800, 30-F11), CD3ε PerCP-eFluor710 (1:400, 17A2), CD69 FITC (1:200, H1.2F3), CD44 eFluor450 (1:400, IM7.8.1), CD62L Alexa 700 (1:800, MEL-14), CD25 APC Alexa 780 (1:200, PC61.5), CD8α APC (1:800, 53-6.7), PD-1 PE (1:200, J43), γδ TCR PE-Cy5 (1:200, GL3), NK1.1 PE (1:200, PK136), CD49b APC (1:400, DX5), CD11b Alexa 700 (1:400, M1/70), CD11c APC Alexa 780 (1:200, N418), MHCII eFluor 450 (1:800, M5/114.15.2), F4/80 PE-Cy5 (1:400, BM8), Ly6C APC (1:800, HK1.4), PDCA-1 PE (1:400, eBio927), and CD103 FITC (1:100, 2E7); from BioLegend, CD49b PerCP-Cy5.5 (1:400, DX5), CD19 PerCP-Cy5.5 (1:200, 6D5), Ly6G PE (1:400, 1A8), and CD206 FITC (1:100, MR5D3); or from Invitrogen, CD4 Qdot 655 (1:100, GK1.5) and B220 Qdot 605 (1:100, RA3-6B2). Cells were then washed once, fixed with BD Cytofix for 30 min on ice, washed again, and stored at 4°C until analysis with an LSRII flow cytometer (BD Bioscience). For detection of FoxP3, cells were prepared after staining for extracellular antigens with the FoxP3 Staining Set (eBioscience) according to the manufacturer's instructions using FoxP3 PE-Cy5 (1:100, FJK-16s, eBioscience).

For analysis of stromal cell populations in mammary tumors, cells were stained for 30 min with CD45 NC605 (1:50, eBioscience), CD31 PE-Cy7 (1:500, eBioscience), PDGFRα biotin (1:250, eBioscience), and PDGFRβ APC (1:250, eBioscience), washed once, then incubated with Streptavidin Alexa 405 (1:500, Invitrogen) for 30 min, and washed again. Cells were then fixed and permeabilized with Cytofix/Cytoperm (BD Biosciences) for 30 min, washed once with Perm/Wash buffer (BD Biosciences),

and incubated with mouse anti-pankeratin Alexa 488 (1:50), rabbit anti-desmin (1:500, Millipore/Upstate), and mouse anti- α -smooth muscle actin Cy3 (α -SMA, 1:500, Sigma-Aldrich). After washing once with Perm/Wash buffer, cells were incubated for 30 min with anti-rabbit Alexa 680 (1:500, Invitrogen), washed again, and stored at 4°C. Prior to analysis on an LSRII, cells were briefly incubated with BD Viaprobe containing 7-aminoactinomycin D (7-AAD) and diploid cells were used for analysis of total cells. All analysis was performed with FlowJo software (Tree Star Inc.).

***Ctsc* mRNA expression**

Following preparation of a single cell suspension, approximately 10^7 cells were Fc blocked with 2.0 μ g/ml of 2.4G2 in PBS containing Live Dead Aqua (1:500, Invitrogen) for 30 min on ice. A 30 min incubation was then performed in PBS containing 2.0 mM EDTA and 1 mg/ml BSA using EpCAM PE-Cy7, CD45 APC-Cy7, PDGFR α PE and CD31 PerCP-Cy5.5. After washing, fluorescence-activated cell sorting (FACS) was performed on live cells using the BD Influx Cell Sorter. cDNA was prepared from isolated cells as described above, and *Ctsc* expression was measured by real-time PCR using the TaqMan system.

3D Organotypic assay

3D organotypic cultures were generated using carcinoma cells isolated as described above from β -actin-GFP transgenic animals (DeNardo et al. 2009). TAMs were purified using the EasySep biotin selection system (Stem Cell Technologies) and biotinylated F4/80 (BioLegend) according to the manufacture's instructions. 5×10^4 TAMs were added to preformed organoids and incubated with or without IL-4 (20 ng/ml) for 48 hrs prior to analysis of acini formation.

Detection of circulating tumor cells

Peripheral blood was removed from anesthetized mice by cardiac puncture, the cellular compartment was isolated by centrifugation, and red blood cells were lysed with PharmLyse (BD Bioscience). Half of the cells were stained for CD45 and pankeratin and analyzed by flow cytometry as described above, while the other half were frozen as a pellet in liquid N₂ for PCR. mRNA was isolated from frozen cells using the RNeasy mini kit (Qiagen), contaminating DNA was removed by DNase I (Invitrogen) digestion, and reverse transcription into cDNA was performed using Superscript III (Invitrogen) according to the manufactures' directions. Real-time PCR for Keratin 18 expression was performed using the TaqMan system (Applied Biosystems) and expression of the PyMT transgene was analyzed via SYBR Green (Invitrogen) using forward primer 5'-TAA GAA GGC TAC ATG CGG ATG GGT-3' and reverse primer 5'-GGC ACC TGG CAT CAC ATT TGT CTT-3' (Integrated DNA Technologies). GAPDH was used as an

internal expression control for each system, with forward primer 5'-AAG TGT GAC GTT GAC ATC CGT-3' and reverse primer 5'-TGC CTG GGT ACA TGG TGG TA-3' used with SYBR Green.

Angiogenesis matrigel plug assay

Matrigel matrix with reduced growth factor composition (BD Biosciences) was diluted 1:1 in cold PBS. PDSC5 cells (Clone 6) or primary NAFs derived from ears of HPV16/CtsC^{-/-} versus HPV16/CtsC^{+/-} mice at 4 months of age were re-suspended at a density of 1.5×10^6 /100 μ l and pre-mixed with diluted Matrigel in a total volume of 300 μ l. Matrigel was injected s.c. in the ventral side by the groin area of 7 week old CtsC^{+/-} and CtsC^{-/-} mice. At day 26 post-injection, Matrigel plugs appeared as lumps on the ventral side of mice. Mice bearing plugs were sacrificed, plugs were recovered and fixed in 10% neutral-buffered formalin and paraffin embedded. The extent of neovascularization was evaluated by staining for rat anti-mouse CD31 (BD biosciences).

Preparation of bone marrow-derived mast cells (BMMC) and stimulation with IgE

BMMC were prepared as previously published (Andreu et al. 2010). Briefly, bone marrow cells were flushed out of femurs of 4-week old CtsC^{+/-} and CtsC^{-/-} mice using a 23-gauge needle. Cells were then cultured in RPMI 1640 supplemented with 10% FBS, 2.0 mM L-glutamine, 100U/ml penicillin, 100 μ g/ml streptomycin, non-essential amino acids, 14.2 mM 2-mercaptoethanol (cRPMI), to which murine recombinant IL3 (for BMMC, 30 ng/ml; PeproTech, Rocky Hill, NJ) was added. Differentiating mast cells were cultured once per week by transferring non-adherent cells and replenishing half of the medium with a fresh one in the presence of IL3 (10 ng/ml). To verify differentiation of BMMC, metachromatic staining was evaluated using toluidine blue and flow cytometric analysis was performed 4 weeks later to assess expression of mast cell markers CD117/c-kit and Fc ϵ R-1 (eBiosciences). Purity was usually >97%. BMMC were used between weeks 4 and 12. All cell cultures were maintained at 37°C in a humidified atmosphere with 5% CO₂. To stimulate BMMC, cells were starved for 4 hr in cRPMI medium in the absence of IL3, followed by culturing at high density (5×10^6 cells/ml) in cRPMI medium containing IL3 (5.0 ng/ml) in combination with IL4 (20 ng/ml; PeproTech) for 4 days. BMMC were then washed, resuspended at 5×10^5 cells/ml in DMEM supplemented with 1.0 % BSA. To eliminate the possibility of non-specific binding of IgE to cell surfaces through Fc γ RII/III, BMMC were incubated with 2.4G2 (10 μ g/ml) for 20 min at 4°C. Cells were then washed and sensitized with 10 μ g/ml anti-dinitrophenol (DNP) IgE (Sigma) for 12 hr at 37°C. To induce cross-linking, BMMC were washed twice and incubated overnight with anti-IgE mAb (1 μ g/ml; Peprotech). Conditioned medium was collected, centrifuged to remove cellular debris, and stored at -70°C for subsequent analysis.

Ethics statement

De-identified human tissue was received from the UCSF Department of Pathology, with patient consent forms obtained at the time of tissue acquisition. Authorization for use of samples was through the UCSF Committee on Human Research (05028310) under “exempt category 4” for individuals receiving de-identified biological specimens.

Supplemental Figure Legends

Supplemental Figure S1: CtsB is not a critical mediator of squamous carcinogenesis. (A) Percentage of CD45⁺ cells in skin assessed by flow cytometry on single cell suspensions from skin of (-) LM, HPV16/CtsB^{-/-}, and littermate HPV16/CtsB^{+/+} mice at 1, 4, and 6 months of age. (B) Flow cytometric analysis of immune cell lineages expressed as percentages of total CD45⁺ leukocyte infiltrates in skin tissue of (-) LM, HPV16/CtsB^{-/-}, and HPV16/CtsB^{+/+} mice. (C) Mast cell infiltration (blue staining) was evaluated by chloroacetate esterase histochemistry in skin of HPV16/CtsB^{-/-} and HPV16/CtsB^{+/+}. (D) Granulocyte infiltration as evaluated by 7/4 immunohistochemistry in skin of HPV16/CtsB^{-/-} and HPV16/CtsB^{+/+} mice. (E) Angiogenic vasculature evaluated by CD31/PECAM-1 immunohistochemistry of in skin sections of (-) LM, HPV16/CtsB^{-/-}, and HPV16/CtsB^{+/+} mice. (F) Keratinocyte hyperproliferation in skin sections of HPV16/CtsB^{-/-} mice as compared to HPV16/CtsB^{+/+} mice as evaluated by quantitation of bromodeoxyuridine (BrdU)-positive keratinocytes (red staining). (G) Lifetime incidence of SCC was determined in HPV16/CtsB^{-/-} as compared to littermate HPV16/CtsB^{+/+} mice. (H) SCC grading in HPV16/CtsB^{-/-} and HPV16/CtsB^{+/+} mice. n>60 mice per group. (A-F) Results shown represent mean ± SEM (n=3-10 mice per group). Values represent average of five high-power fields of view per mouse and five mice per category. Representative images of HPV16/CtsB^{-/-} and HPV16/CtsB^{+/+} mouse skin at 4 months of age are shown. FOV, field of view; solid line, epidermal-dermal interface; epidermis, e; dermis, d; scale bar, 50 μm.

Supplementary Figure S2: Increased CtsC protein and activity during neoplastic progression. (A) Quantitation of CtsC protein levels from whole tissue by ELISA in negative littermate (-LM) ear skin and hyperplastic (1m), early dysplastic (4m), and carcinoma (SCC) tissue of HPV16 mice. n=3-4 mice per group. Significance was determined by an unpaired *t* test with * p < 0.05, ** p < 0.01. (B) FY01 labeling of enzymatically active CtsC within total cell extracts derived from negative littermate (-LM) ear skin and hyperplastic (1m), early dysplastic (4m), late dysplastic (6m), and carcinoma (SCC) tissue of HPV16 mice. CtsC^{-/-} tissue and the inhibitor JCP410 served as negative controls.

Supplementary Figure S3: Stromal and epithelial cells express CtsC. CtsC mRNA levels in stromal cells isolated from dysplastic skin of HPV16/CtsC^{+/+} mice (6 months of age, dysplasia) (A) and mammary adenocarcinoma (100-110 days old) from MMTV-PyMT mice (B) as determined by real-time PCR. Expression is shown relative to *Tbp* (TATA box binding protein). n=4-8 mice per group.

Supplementary Figure S4: CtsC expression is prominent in macrophages in metastatic-bearing lungs.

Low CtsC expression levels were visualized in tissue sections by confocal microscopy within metastatic foci (Keratin⁺, bottom panels), but not CD31⁺ endothelial cells, SMA⁺ pericytes (2nd from bottom), or fibroblasts (PDGFR α ⁺, middle panels). High expression of CtsC was observed in CD45⁺ leukocytes (top panels), including F4/80⁺ macrophages (2nd from top).

Supplementary Figure S5: CtsC expression in human skin SCC and breast carcinomas.

Immunohistochemistry for CtsC (brown staining) in human SCC (A) and breast carcinomas (B). Images were obtained from The Human Protein Atlas (www.proteinatlas.org). Areas of the tumor (t) and stroma (s) are indicated as reference points.

Supplementary Figure S6: CtsC expression affects leukocyte infiltration and keratinocyte proliferation.

Quantitative evaluation of infiltrating neutrophils (A) and mast cells (B) following 7/4 immunohistochemistry (IHC) and toluidine blue histochemistry, respectively, in (-LM), HPV16/CtsC^{+/-}, and HPV16/CtsC^{-/-} mice at 1, 4, and 6 months of age. (C) Representative staining for bromodeoxyuridine (BrdU) incorporation by keratinocytes (red staining) at distinct stages of premalignant progression in ear tissue of HPV16/CtsC^{+/-}, and HPV16/CtsC^{-/-} mice at 1, 4, and 6 months of age. n=4-8 mice per group (A-B). Significance was determined by an unpaired *t* test with * *p* < 0.05, ** *p* < 0.01, *** *p* < 0.001.

Supplementary Figure S7: CtsC expression does not influence macrophage-dependent lung metastasis.

(A) Quantitation of the number of metastatic foci per lung for MMTV-PyMT mice at end stage with representative lung sections depicting metastatic tumor burden at end stage visualized by H&E staining shown on the right. n=35-50 mice per group. (B) Real-time PCR quantitation of *Keratin 18* and *PyMT* mRNA expression from circulating cells from MMTV-PyMT/CtsC^{+/-} (blue) and MMTV-PyMT/CtsC^{-/-} (red) animals. Expression is normalized with the control gene *Tbp* (TATA box binding protein). (C) Quantitation of circulating cytokeratin⁺CD45⁻ cells by flow cytometry from MMTV-PyMT/CtsC^{+/-} (blue) and MMTV-PyMT/CtsC^{-/-} (red) animals. (D) Purification and analysis of polarization markers. Tumor-associated macrophages (TAMs) from MMTV-PyMT animals were purified to >90% via magnetic beads and analyzed for marker expression by flow cytometry. (E) 3D organotypic invasion assay with non-polarized or interleukin-4 polarized TAMs from both MMTV-PyMT/CtsC^{+/-} (blue) and MMTV-PyMT/CtsC^{-/-} (red) mice. Representative organoids (green) with TAMs (red) are shown on the right, while quantitation of the percent of organoids displaying invasive acini greater than half their diameter is shown on the left. Data represents an average of 4 wells per group. One of two representative experiments is

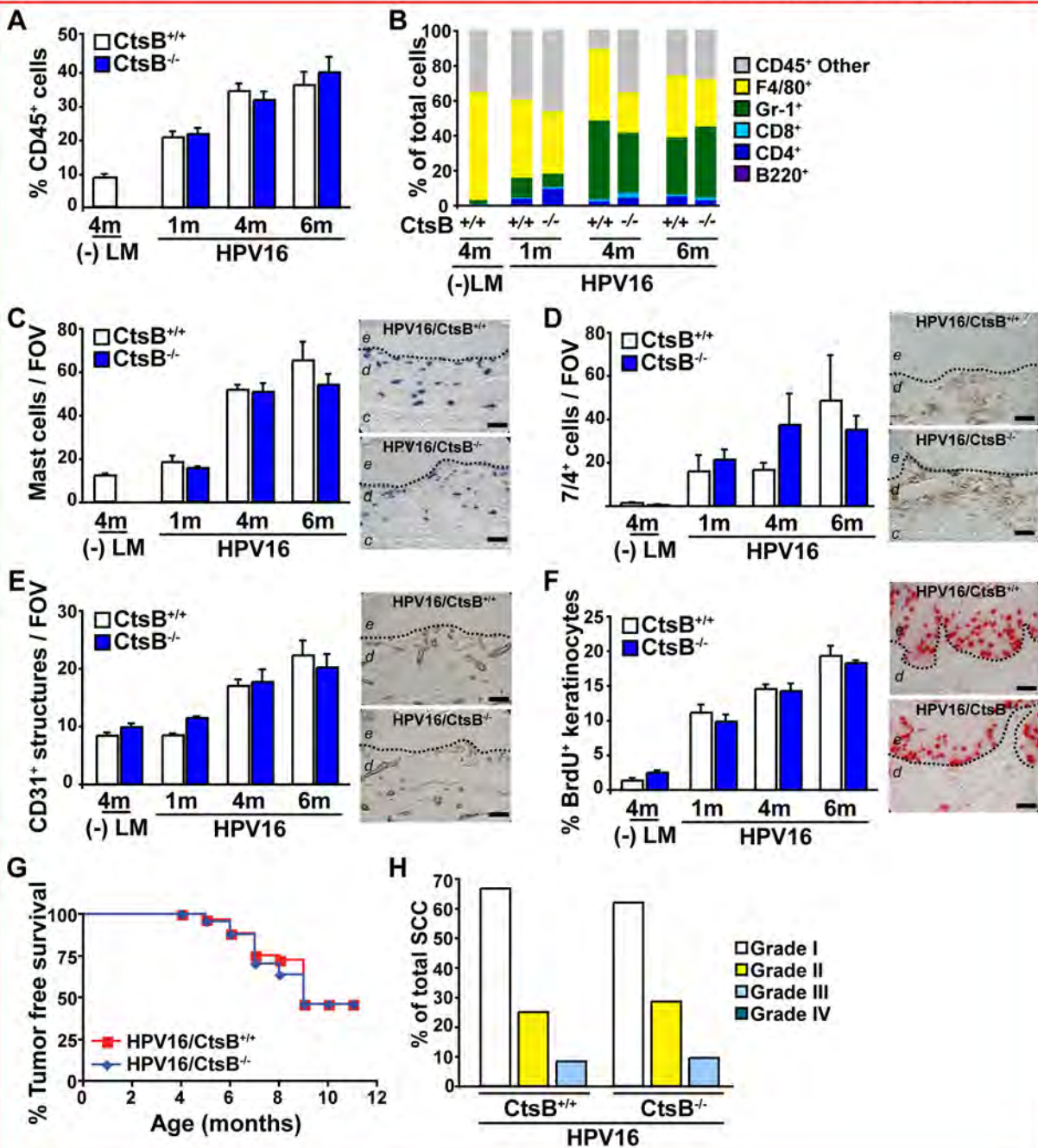
shown.

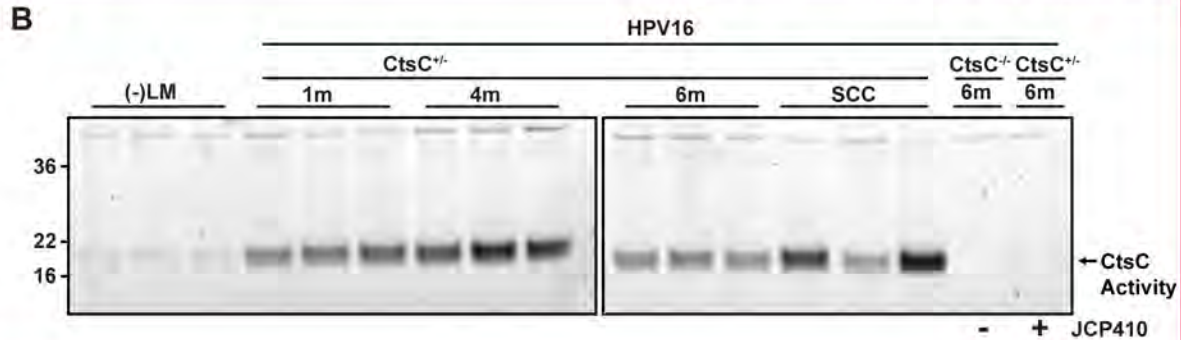
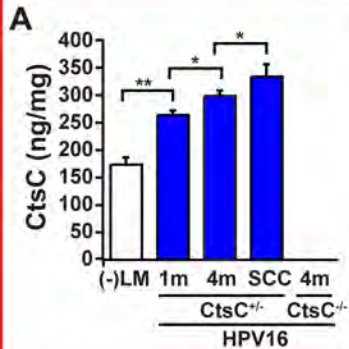
Supplemental Figure S8: MMP9 levels and enzymatic activity in the absence of CtsC during HPV16 premalignant progression. (A-C) Pro-MMP9, MMP9, and TIMP1 protein levels in skin extracts from negative littermates (-LM), HPV16/CtsC^{+/-}, and HPV16/CtsC^{-/-} mice at 1, 4, and 6 months of age assessed by ELISA. (D) Gelatinolytic activity in tissue extracts measured by enzyme solution assay. Values represent average change in relative fluorescence units (RFU)/min/μg tissue protein. (E) Tissue lysates from (-LM), HPV16/CtsC^{+/-}, and HPV16/CtsC^{-/-} mice at 1, 4, and 6 months of age were evaluated for presence of enzymatic activities corresponding to pro- and active molecular weight forms of MMP9 and MMP2 by gelatin substrate zymography. (A-D) n=3-4 mice per group. Significance was determined by an unpaired *t* test with * *p* < 0.05, ** *p* < 0.01 for differences between age-matched HPV16/CtsC^{-/-} versus HPV16/CtsC^{+/-}.

Supplemental Figure S9: Stromal expression of CtsC is necessary for angiogenesis and tumor growth in the skin. (A) PDSC5 clone 2 (PDSC5.2) tumor cells were injected s.c. into CtsC^{-/-} versus CtsC^{+/-} syngeneic FVB/n mice. n=5 mice per group. Significance between CtsC^{-/-} versus CtsC^{+/-} hosts was determined by an unpaired *t* test with * *p* < 0.05. (B) Expression of mature form of CtsC in PDSC5.6 and PDSC5 clone 2 (PDSC5.2) was verified by western blotting analysis. Splenocytes were used as a positive control. (C) Blood vessels were evaluated by CD31 IHC in tumor tissue from (A) at day 42 following PDSC5.2 implantation into CtsC^{+/-} versus CtsC^{-/-} mice. Values represent average of five high-power fields of view per mouse. n=3-8 tumors per group. (D) PDSC5 (clone 6) cells were injected as matrigel plugs into CtsC^{+/-} (blue) or CtsC^{-/-} (red) mice. Neovascularization was evaluated by CD31 IHC at 26 days following inoculation. n=5-6 mice per group. (C-D) Significance was determined by an unpaired *t* test with *** *p* < 0.001. (E) HPV16/CtsC^{+/-}-derived NAF isolated at 1 month of age were not sufficient to restore tumor growth in CtsC^{-/-} mice. PDSC5.6 cells alone (blue) or admixed with HPV16/CtsC^{+/-}- (orange) or HPV16/CtsC^{-/-}-derived NAF (green) were injected s.c. into CtsC^{+/-} (circle) or CtsC^{-/-} (square) at a ratio of 3:1 (PDSC5:NAF). n=8-10 mice per group. Significance between PDSC5 cells in combination with NAF derived from HPV/CtsC^{+/-} mice versus PDSC5 cells alone in CtsC^{+/-} hosts was determined by an unpaired *t* test with * *p* < 0.05. (F) HPV16/CtsC^{+/-}- or HPV16/CtsC^{-/-}-derived NAF isolated at 4 months of age were injected as matrigel plugs into CtsC^{+/-} (blue) or CtsC^{-/-} (red) mice. Neovascularization was evaluated by CD31 IHC at 26 days following inoculation. n=4-5 mice per group. Significance was determined by an unpaired *t* test with ** *p* < 0.01, *** *p* < 0.001. (G) PDGFRα⁺ NAF were isolated by FACS from HPV16/CtsC^{+/-} mice at 1 and 6 months of age, or from negative littermate (-LM) controls at 1 month of age,

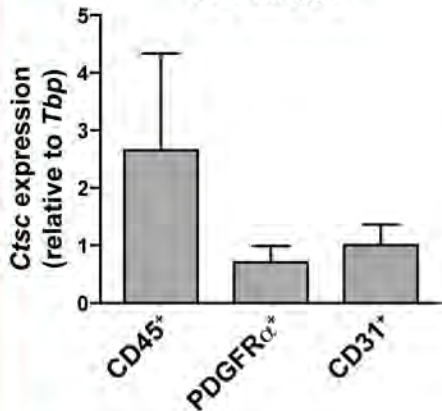
and analyzed by real time PCR for expression of *Ctsc*. Data is shown relative to *Tbp* expression with n=4 mice per group. **(H)** Transplantation of lethally irradiated *CtsC*^{+/-} and *CtsC*^{-/-} mice with GFP⁺ bone marrow-derived cells was confirmed by evaluating peripheral blood leukocytes (PBL) for expression of GFP by flow cytometry. PBL isolated from GFP⁺ FVB/n mice were used as a positive control. **(I)** Growth kinetics of tumors shown in **Fig. 5G**. n=3-5 mice per category.

Supplemental Figure S10: Expression of CTSC in human head and neck carcinomas. Relative expression of *CTSC* in human head and neck carcinomas compiled and displayed by box plot using Oncomine (www.oncomine.org). The number of samples is shown in parenthesis. Significance was determined by a Student's t-test. Datasets utilized include: Estilo Head-Neck, Toruner Head-Neck, Sengupta Head-Neck, He Thyroid, and Ginos Head-Neck.

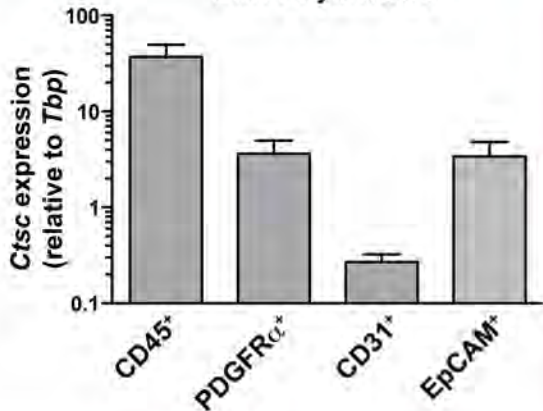




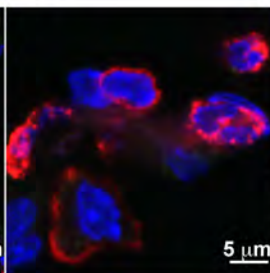
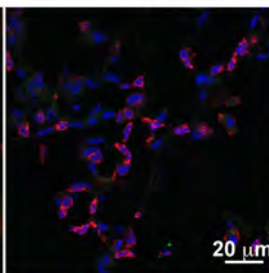
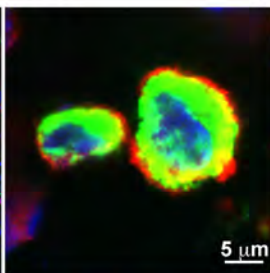
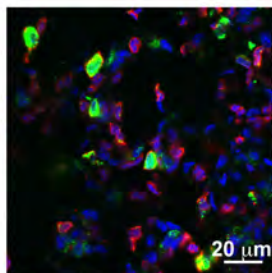
A

HPV16/CtsC^{+/+}

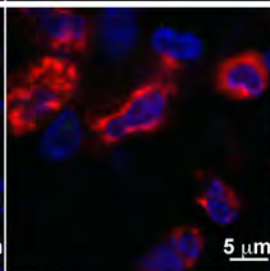
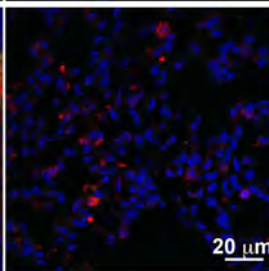
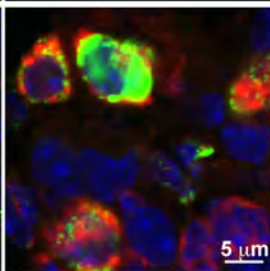
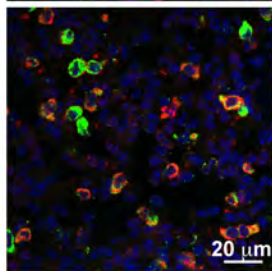
B

MMTV-PyMT/CtsC^{+/+}

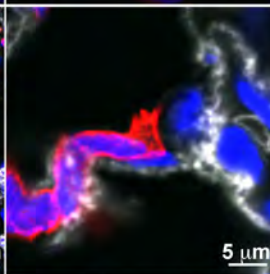
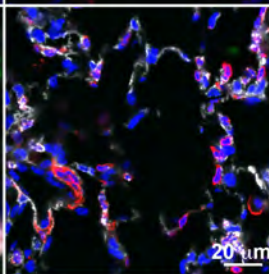
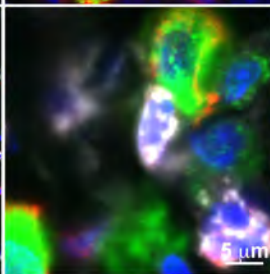
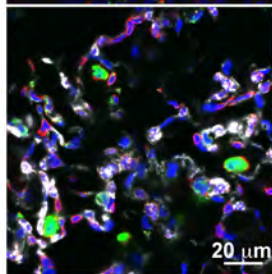
Metastatic Lungs

PyMT CtsC^{+/-}PyMT CtsC^{-/-}CtsC
CD45
DAPI

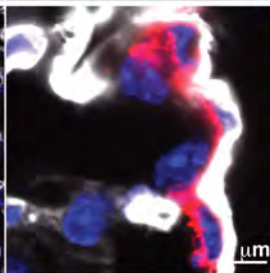
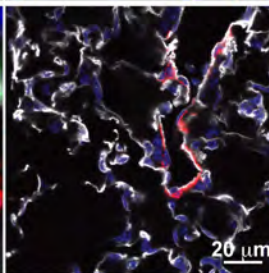
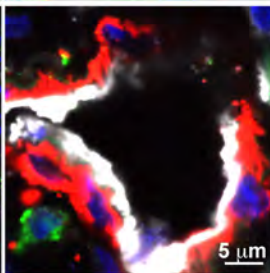
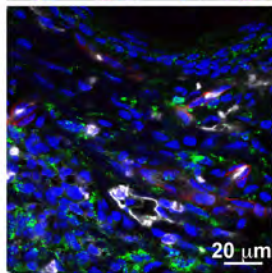
Leukocytes

CtsC
F4/80
DAPI

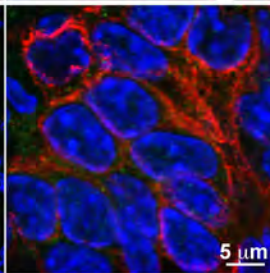
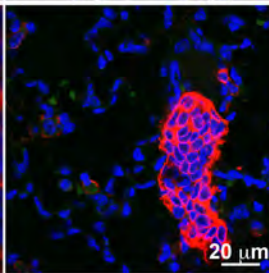
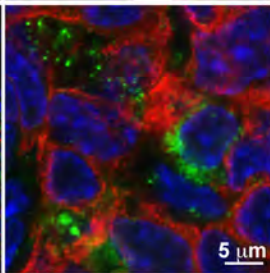
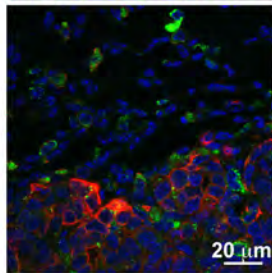
Macrophages

CtsC
CD45
PDGFR α
DAPI

Fibroblasts

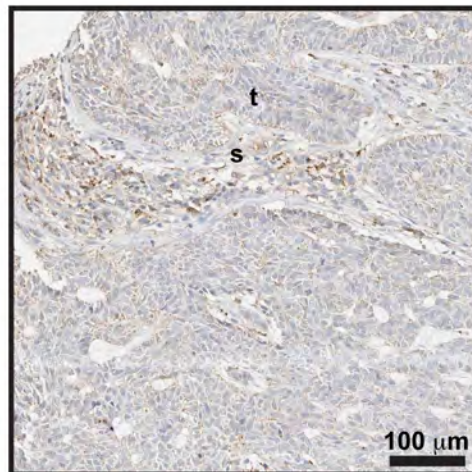
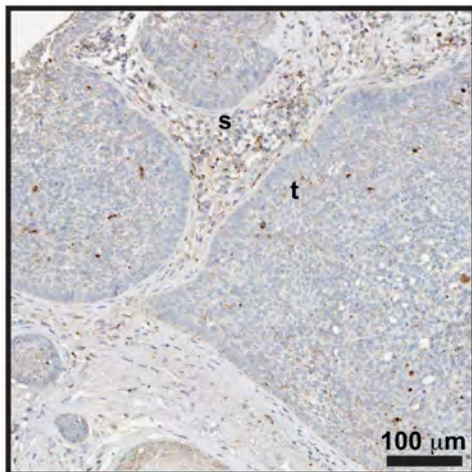
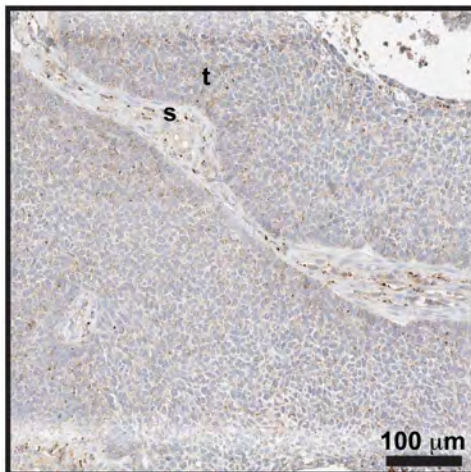
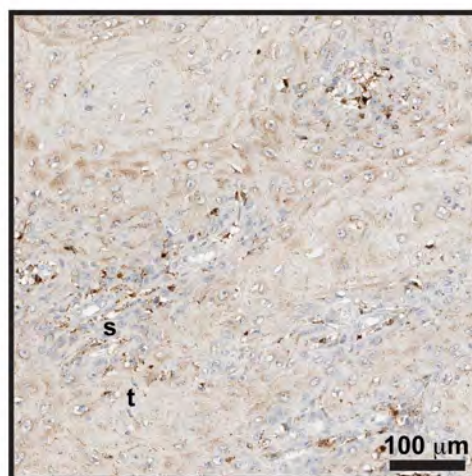
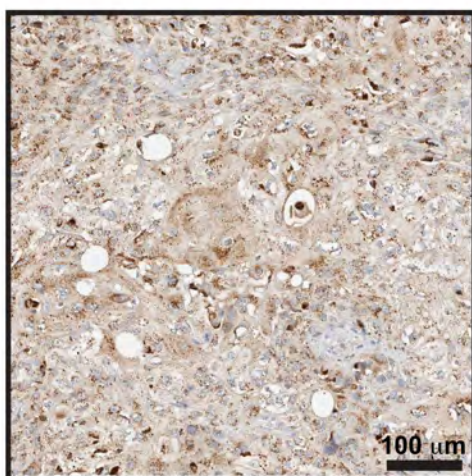
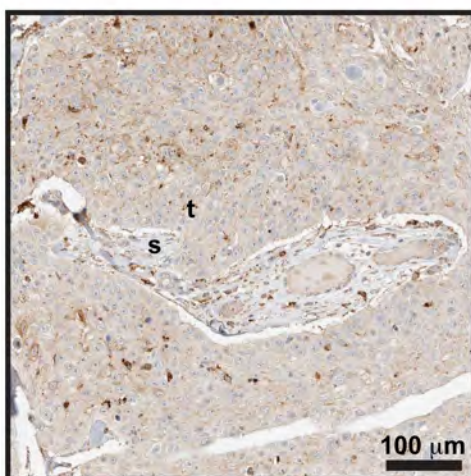
CtsC
SMA
CD31
DAPI

Endothelial / Mural

CtsC
Keratin
DAPI

Epithelial

A



B

